

Adjuvant lipidoid-substituted lipid nanoparticles augment the immunogenicity of SARS-CoV-2 mRNA vaccines

Received: 13 July 2022

Accepted: 17 April 2023

Published online: 26 June 2023

 Check for updates

Xuexiang Han^{1,16}, Mohamad-Gabriel Alameh^{2,3,4,16}, Kamila Butowska^{1,5}, James J. Knox⁶, Kendall Lundgreen⁷, Majed Ghattas⁸, Ningqiang Gong¹, Lulu Xue¹, Ying Xu⁹, Marc Lavertu⁸, Paul Bates⁷, Junchao Xu¹⁰, Guangjun Nie¹⁰, Yi Zhong¹¹, Drew Weissman^{2,3}✉ & Michael J. Mitchell^{1,3,12,13,14,15}✉

Lipid nanoparticle (LNP)-formulated messenger RNA (mRNA) vaccine are a promising platform to prevent infectious diseases as demonstrated by the recent success of SARS-CoV-2 mRNA vaccines. To avoid immune recognition and uncontrolled inflammation, nucleoside-modified mRNA is used. However, such modification largely abrogates the innate immune responses that are critical to orchestrating robust adaptive immunity. Here we develop an LNP component—an adjuvant lipidoid—that can enhance the adjuvant activity of mRNA-LNP vaccines. Our results show that partial substitution of ionizable lipidoid with adjuvant lipidoid not only enhanced mRNA delivery, but also endowed LNPs with Toll-like receptor 7/8-agonistic activity, which significantly increased the innate immunity of the SARS-CoV-2 mRNA-LNP vaccine with good tolerability in mice. Our optimized vaccine elicits potent neutralizing antibodies against multiple SARS-CoV-2 pseudovirus variants, strong Th1-biased cellular immunity, and robust B cell and long-lived plasma cell responses. Importantly, this adjuvant lipidoid substitution strategy works successfully in a clinically relevant mRNA-LNP vaccine, demonstrating its translational potential.

The coronavirus disease 2019 (COVID-19), caused by severe acute respiratory syndrome coronavirus 2 (SARS-CoV-2), has resulted in a global health crisis with over six million casualties thus far (<https://coronavirus.jhu.edu/map.html>). Vaccines have proved to be efficacious at reducing the morbidity and mortality of this infectious disease. Currently, several vaccine modalities, including messenger RNA (mRNA) vaccines, antigen-expressing adenovirus, inactivated virus and subunit vaccines, are either approved or under clinical development¹. Among the different platforms, mRNA vaccines not only demonstrate superior ability to elicit both neutralizing antibody (NAb) and T cell responses against multiple SARS-CoV-2 variants², but also offer low production costs with short development and manufacturing times^{3,4}.

Although mRNA was discovered in 1961 (ref. 5), due to its susceptibility to enzymatic degradation, inefficient *in vivo* delivery and high innate immunogenicity, its use in vaccine development has been hampered until recently⁶. The first two challenges have been overcome by the incorporation of mRNA into a delivery system that can protect it from degradation and escort it across various biological barriers^{7–9}. Notably, four-component lipid nanoparticles (LNPs) comprising ionizable lipid (or lipidoid), phospholipid, PEGylated lipid and cholesterol are the most clinically advanced mRNA delivery platform as exemplified by Pfizer/BioNTech's BNT162b2 and Moderna's mRNA-1273 vaccines⁸. The last challenge is addressed through the incorporation of naturally occurring nucleosides such as 1-methylpseudouridine (m1ψ) into the

A full list of affiliations appears at the end of the paper. ✉ e-mail: dreww@upenn.edu; mjmitch@seas.upenn.edu

in vitro transcribed mRNA sequence to avoid its recognition by pattern recognition receptors^{10,11}. Despite its improved tolerability and translation, the use of nucleoside-modified mRNA largely compromises the innate immune responses and weakens the activation of dendritic cells (DCs, the major recipient cells of mRNA-LNP vaccines¹²), a process that is critical to mounting a strong adaptive immunity to vaccination^{3,13}.

Interestingly, we and others have found that certain LNPs possess intrinsic adjuvant activity that can promote the induction of cellular and humoral immune responses of mRNA and subunit vaccines^{14–16}. However, the adjuvanticity of LNPs is variable based on the lipidoid used and is generally weak and non-specific¹⁴. Toll-like receptor agonists (TLRAs) are potent adjuvants, which activate DCs to present antigen, express co-stimulatory molecules and produce selective cytokines (for example, tumour necrosis factor- α (TNF- α)) that effectively stimulate the transition from innate to adaptive immunity¹⁷. Several small-molecule TLRAs with high specificity have been approved for immunomodulation¹⁸, including imidazoquinoline-based TLR7/8 agonists (for example, imiquimod)¹⁹. The incorporation of fatty acid-modified TLRAs in antigen-loaded liposomes or NPs has been demonstrated to enhance the magnitude and duration of adaptive immune responses^{20,21}. We hypothesized that formulation of a rationally designed TLRa-derived ionizable lipidoid into LNPs could further augment the immunogenicity of mRNA-LNP vaccines due to the accessorial adjuvant properties.

In this study, we chemically synthesized an LNP component—an adjuvant lipidoid—based on a TLR7/8 agonist. Unlike previous studies in which the TLRa was typically conjugated to macromolecules (for example, lipids, peptides and polymers) through acylation^{22–24}, we applied the ring-opening reaction between an amine-bearing TLRa and an alkyl epoxide to yield a tertiary amine-containing ionizable lipidoid that can complex with and deliver negatively charged mRNA into cells²⁵. We optimized the formulation of this adjuvant lipidoid-incorporated SARS-CoV-2 mRNA-LNP vaccine and systematically evaluated its innate and adaptive immune responses (Fig. 1).

Synthesis of adjuvant lipidoid and polyamine-based lipidoids

Adjuvant lipidoid C12-TLRa was synthesized by the ring-opening reaction between amine-containing TLR7/8 agonist 1 and C12 epoxide (Fig. 2a)²⁵. The purity and structure of C12-TLRa were verified by liquid chromatography–mass spectrometry and proton NMR (Supplementary Figs. 1 and 2). Structural simulation via computational analysis demonstrated that C12-TLRa could form multiple interactions with TLR7 receptor (for example, hydrogen bonding with Asp⁵⁵⁵ and Thr⁵⁸⁶ and π – π stacking with Phe⁴⁰⁸) at its first binding site that were similar to TLR7/8 agonist 1 (Supplementary Fig. 3)^{26,27}, suggesting that such modification barely interrupts the agonist–receptor interaction. The TLR7-agonistic activity of C12-TLRa was further verified on HEK-Blue reporter cells stably expressing the TLR7 receptor. As a positive control, TLR7/8 agonist 1 exhibited a biphasic dose–response profile of TLR7-agonistic activity characterized by an initial dose-dependent increase followed by a decrease of analytes (Supplementary Fig. 4), which was also observed by others^{28,29}. However, monotonically dose-dependent TLR7-agonistic activity of C12-TLRa was observed at the same dose range, indicating that C12-TLRa has a more predictable pharmaceutical property despite its reduced potency.

Next, adjuvant lipidoid, phospholipid, cholesterol and 1,2-dimyristoyl-rac-glycero-3-methoxypolyethylene glycol-2000 (DMG-PEG) at a molar ratio of 35:16:46.5:2.5 were formulated into C12-TLRa LNP along with mRNA using microfluidic mixing (Supplementary Table 1)³⁰. In this formulation, 1,2-dioleoyl-*sn*-glycero-3-*p* phosphoethanolamine was used as it has generally exhibited greater mRNA delivery than other phospholipids such as 1,2-distearoyl-*sn*-glycero-3-phosphocholine^{31,32}. The mRNA encapsulation efficiency was determined to be ~75%, suggesting that this adjuvant lipidoid is able to complex with and encapsulate negatively

charged mRNA into LNPs. m1 ψ -modified firefly luciferase mRNA (mLuc)-encapsulated C12-TLRa LNP was then used to treat DC2.4 dendritic cells. Although free mLuc was unable to transfect cells, C12-TLRa LNP demonstrated dose-dependent mRNA transfection (Fig. 2b), showing that adjuvant lipidoid can successfully deliver mRNA into cells. To further evaluate the potency of C12-TLRa, it was compared with a series of polyamine-derived lipidoids synthesized using the same chemistry (Fig. 2c and Supplementary Fig. 5)²⁵. It should be noted that some polyamine-derived lipidoids in this library exhibited potent RNA delivery in previous studies^{25,31}. In vitro mLuc transfection results demonstrated that C12-TLRa had a relatively low transfection ability, especially when compared with the top performer C12-I13 (Fig. 2d).

Optimization and characterization of LNPs

Since adequate antigen expression is favourable for mRNA vaccines, we decided to partially replace the ionizable lipidoid in C12-I13 LNP with C12-TLRa to endow the LNPs with TLR7/8-agonistic properties without compromising mRNA delivery. Therefore, a series of C12-I13/TLRa LNP with an increased C12-TLRa substitution (1–17.5 mol%) was formulated and subjected to in vitro screening. Interestingly, along with the increased substitution with C12-TLRa, the mRNA transfection efficiency of C12-I13/TLRa LNP first increased and then decreased (Fig. 2e). The highest transfection was achieved by C12-I13/TLRa LNP with 5 mol% of C12-TLRa, and this was chosen for subsequent studies.

The adjuvant activity of mRNA-loaded C12-I13/TLRa LNP was then verified in HEK-Blue reporter cells. Whereas C12-I13 LNP possessed no TLR7-agonistic activity, C12-I13/TLRa LNP exhibited dose-dependent TLR7-agonistic activity (Fig. 2f). Consequently, C12-I13/TLRa LNP stimulated proinflammatory cytokine TNF- α production in DC2.4 cells in a dose-dependent manner, which significantly outperformed C12-I13 LNP (Supplementary Fig. 6). To further confirm the general applicability of this strategy, DLin-MC3-DMA (MC3) LNPs and adjuvant lipidoid-substituted MC3 LNP (that is, MC3/TLRa LNP), and SM-102 LNP and adjuvant lipidoid-substituted SM-102 LNP (that is, SM-102/TLRa LNP) were formulated and tested (Supplementary Table 1). Consistently, MC3/TLRa LNP and SM-102/TLRa LNP, but not MC3 LNP or SM-102 LNP, showed obvious TLR7-agonistic activity (Supplementary Fig. 7). These results suggest that the substitution of partial lipidoid with C12-TLRa can endow LNPs with adjuvant activity irrespective of LNP formulation.

Next, the physicochemical properties of the C12-I13/TLRa LNP were characterized. This LNP had a hydrodynamic diameter of approximately 52 nm and a polydispersity index (PDI) of 0.127 (Supplementary Table 1). Additionally, it had a neutral surface charge in phosphate-buffered saline (PBS, pH 7.4), and its apparent pK_a was determined to be 6.42 by conducting a 6-(*p*-toluidinyl) naphthalene-2-sulfonic acid (TNS) assay over the range of pH 2–12 (ref. 33), which meet the criteria for potent in vivo mRNA delivery^{34,35}. The encapsulation efficiency of mRNA in C12-I13/TLRa LNP was >93%. After 1 month of storage at 4 °C, we observed minimal changes in all major LNP physicochemical parameters (Supplementary Fig. 8), indicating the good stability of this LNP. Representative transmission electron microscopy (TEM) and cryogenic electron microscopy (cryo-EM) images showed that C12-I13/TLRa LNP had a uniform, compact spherical structure (Fig. 2g and Supplementary Fig. 9a). C12-I13 LNP without C12-TLRa substitution had very similar parameters and morphology (Supplementary Table 1, and Supplementary Figs. 8 and 9), suggesting that substitution with 5% C12-TLRa does not alter the physicochemical properties or affect the stability of these LNPs.

In vitro mRNA delivery and DC activation

We next systematically investigated the in vitro mRNA delivery and adjuvant activity of C12-I13/TLRa LNP. Both C12-I13 LNP and C12-I13/TLRa LNP exhibited dose-dependent mLuc transfection in DC2.4 cells (Fig. 3a); however, in line with Fig. 2e, C12-I13/TLRa LNP consistently outperformed C12-I13 LNP at any mRNA dose tested. Similarly, in

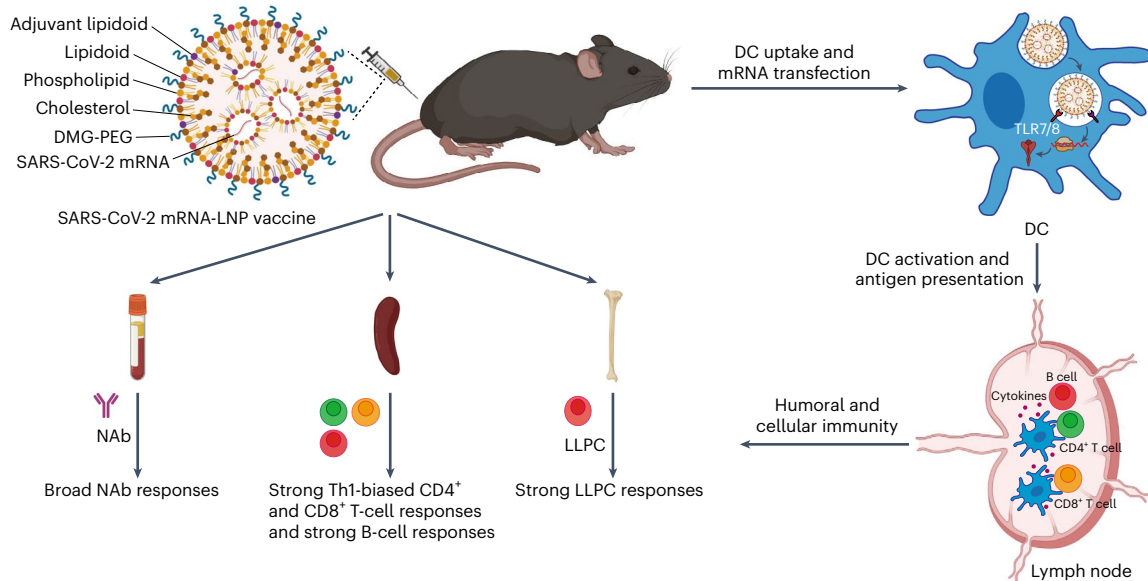


Fig. 1 | Adjuvant lipidoid-substituted SARS-CoV-2 mRNA-LNP vaccine and its proposed mechanism of action to elicit potent adaptive immunity.

SARS-CoV-2 mRNA-LNP vaccine is formulated with adjuvant lipidoid, lipidoid, phospholipid, DMG-PEG and cholesterol, along with m1 ψ -modified SARS-CoV-2 mRNA encoding the diproline-modified spike glycoprotein. After injection, the vaccine is internalized by DCs, where adjuvant lipidoid agonizes endosomally

localized TLR7/8 to activate DCs and mRNA is translated into spike antigen that is processed and presented by DCs. After migration into the draining lymph node, activated DCs orchestrate robust adaptive immunity together with CD4⁺ T, CD8⁺ T and B cells, including NAb responses, Th1-biased CD4⁺ and CD8⁺ T cell responses, B cell responses and LLPC responses.

primary murine bone marrow-derived dendritic cells (BMDCs) and human monocyte-derived dendritic cells (MoDCs), C12-113/TLRa LNP consistently exhibited higher mRNA transfection efficiency than C12-113 LNP (Fig. 3b,c). No obvious cytotoxicity towards these cells was observed at the dose tested for both LNPs (Supplementary Fig. 10). Moreover, MC3/TLRa LNP and SM-102/TLRa LNP significantly outperformed their respective counterpart in terms of mLuc delivery (Supplementary Fig. 11). These results suggest that C12-TLRa substitution can increase LNP-mediated mRNA delivery in vitro irrespective of LNP formulation.

To investigate the mechanism of enhanced mRNA transfection following C12-TLRa incorporation, we studied the endosomal escape of LNPs. Lipid-like fluorescent dye 3,3'-di-octadecyloxycarbocyanine perchlorate (DiO)-labelled LNPs were used to treat DC2.4 cells and their subcellular distribution was visualized after endo/lysosomes and nuclei were stained (Fig. 3d). In C12-113 LNP-treated cells, there were large yellow spots, indicating severe entrapment of C12-113 LNP (green) inside endo/lysosomes (red). In contrast, C12-113/TLRa LNP-treated cells exhibited more diffuse green signal across the cytoplasm, suggesting its more efficient escape from endo/lysosomes. This observation was further supported by the quantification of LNP endosomal escape. Additionally, similar results were obtained when LNPs encapsulating Cy5-tagged mRNA were used for this endosomal escape study (Supplementary Fig. 12). These results suggest that C12-TLRa substitution enhances endosomal escape of LNPs, which could explain the enhanced mRNA transfection (Fig. 3a-c). Since multiple interactions are predicted between C12-TLRa and TLR7 based on the molecular simulation result (Supplementary Fig. 3), it is reasonable to assume that the strong affinity between the incorporated C12-TLRa and endosomal TLR7/8 could reinforce the physical interaction between LNPs and the endosomal membrane, which leads to enhanced endosomal escape (Fig. 3e).

Next, we studied the immunostimulatory effect of C12-113/TLRa LNP carrying m1 ψ -modified SARS-CoV-2 mRNA encoding the diproline-modified spike glycoprotein. Notably, the coding sequence of this nucleoside-modified mRNA is identical to the mRNA used in two US Food and Drug Administration-approved vaccines (mRNA-1273

and BNT162b2)³⁶. Since TLR7/8 agonist can stimulate DC maturation and proinflammatory cytokine release, we analysed matured DCs (CD80⁺CD86⁺) using flow cytometry and measured TNF- α , interleukin (IL)-12p70 and IL-1 β secretion using enzyme-linked immunosorbent assay (ELISA) at 24 h post-transfection. As expected, C12-113/TLRa LNP markedly increased the percentage of matured DCs in DC2.4 cells, BMDCs and MoDCs (Fig. 3f-h and Supplementary Fig. 13). In contrast, C12-113 LNP only modestly induced DC maturation. Moreover, C12-113/TLRa LNP stimulated a significant increase of TNF- α , IL-12p70 and IL-1 β levels compared to C12-113 LNP in DC2.4 cells, BMDCs and MoDCs (Fig. 3i-k). Altogether, these results suggest that C12-TLRa substitution can greatly enhance the adjuvanticity of LNPs and DC activation.

In vivo mRNA transfection and innate immune responses

We next explored whether increased mRNA transfection and innate immune responses by adjuvant lipidoid-substituted LNPs could be reproduced in vivo. C57BL/6 mice were subcutaneously (s.c.) immunized at the tail bases of mice with mLuc-loaded C12-113 LNP or C12-113/TLRa LNP, and luciferase expression was visualized by in vivo bioluminescence imaging at 6 and 24 h post-treatment (Fig. 4a). Both LNPs mainly transfected injection sites, and could also transfect inguinal lymph nodes (iLNs). In line with in vitro transfection results, C12-113/TLRa LNP achieved greater mRNA transfection than C12-113 LNP at both injection sites and iLNs (Fig. 4a).

To avoid systemic toxicity, it is important to spatially restrict adjuvant activity and mRNA transfection to the sites of vaccine administration and draining lymph nodes³⁷. Therefore, we studied the distribution and transfection of LNPs in major organs and iLNs at 24 h post-injection of lipid-like fluorescent dye 1,1'-di-octadecyl-3,3,3',3'-tetramethylindot ricarbocyanine iodide (DiR)-labelled, mLuc-loaded LNPs. Ex vivo fluorescence and luminescence imaging confirmed that no obvious accumulation and transfection in major organs (liver, heart, spleen, lung and kidney) were observed for either LNP (Fig. 4b). Interestingly, although these two LNPs achieved comparable accumulation amounts in iLNs based on the fluorescence quantification (Fig. 4c), C12-113/TLRa LNP

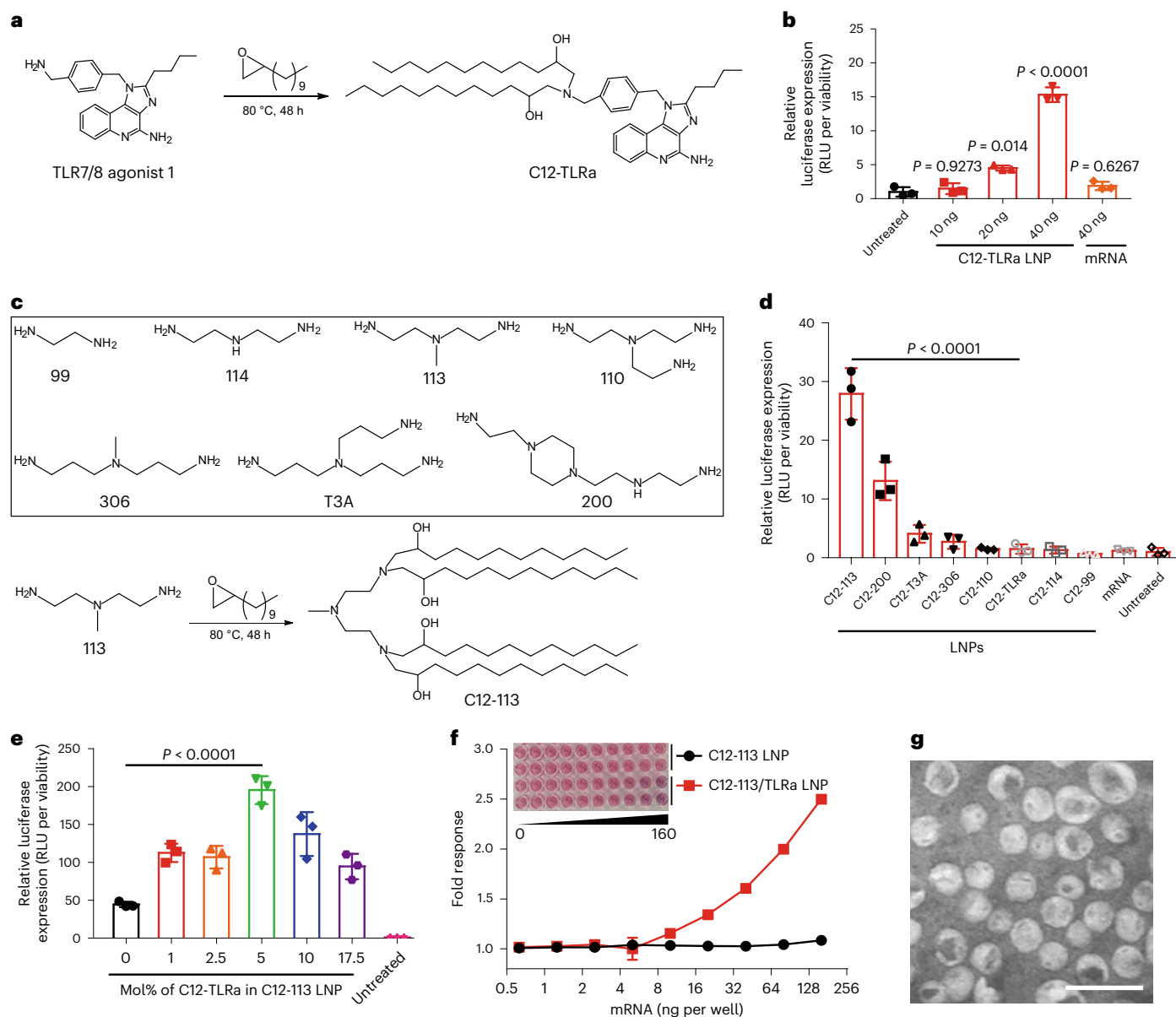


Fig. 2 | Synthesis and characterization of lipidoids and LNPs. a, Synthesis of adjuvant lipidoid C12-TLRa by ring-opening reaction between TLR7/8 agonist 1 and C12 epoxide. **b**, C12-TLRa LNP-mediated mLuc delivery ($n = 3$). DC2.4 cells were treated with mLuc-loaded C12-TLRa LNP (10–40 ng per well) or free mRNA (40 ng per well) for 24 h. **c**, Polyamines and the representative synthesis of polyamine-derived lipidoid C12-113. **d**, Comparison of C12-TLRa with polyamine-derived lipidoids for in vitro mLuc delivery ($n = 3$). DC2.4 cells were treated with different mLuc-loaded LNPs (10 ng per well) or free mRNA (10 ng per well) for 24 h. **e**, Optimization of C12-113/TLRa LNP formulation ($n = 3$). DC2.4 cells were treated with mLuc-loaded C12-113/TLRa LNP (10 ng per well) with

1–17.5 mol% of C12-TLRa substitution for 24 h. **f**, TLR7-agonistic activity of LNPs measured in HEK-Blue reporter cells ($n = 2$). HEK-Blue reporter cells expressing TLR7 were treated with LNPs at different mRNA concentrations in HEK-Blue Detection medium in a 96-well plate for 24 h. The plate was photographed and the absorbance was measured at 650 nm. Data are presented as fold changes relative to untreated cells. x axis scale of the inset is in nanograms per well. **g**, A representative TEM image of C12-113/TLRa LNP from three independent experiments. Scale bar, 100 nm. Data are presented as mean \pm s.d. **b, d, e**, One-way ANOVA with Tukey's correction. Source data are provided as a Source Data file.

enabled stronger mRNA transfection in iLNs than C12-113 LNP, which was in line with in vivo ventral luminescence imaging (Fig. 4a). These results also correlate well with in vitro mRNA transfection (Fig. 3a–c). Moreover, C12-113/TLRa LNP-mediated enhanced mRNA expression at both the injection site and iLNs was highly reproducible from different LNP batches (Supplementary Fig. 14). Finally, the duration and translational kinetics of LNP-formulated mRNA was investigated. C12-113/TLRa LNP enabled more durable (over 14 days) and consistently stronger mRNA expression at the injection site than C12-113 LNP (Supplementary Fig. 15). Such long-lasting expression is attributed to the enhanced translational capacity and biological stability of mRNA as a result of

nucleoside modification and LNP formulation³⁸. Together, these results suggest that C12-TLRa substitution can greatly enhance the expression of LNP-formulated mRNA at both injection sites and draining lymph nodes with minimal systemic off-target distribution or expression.

To assess in vivo innate immune responses, iLNs were harvested from mice at 24 h post-immunization with SARS-CoV-2 mRNA-loaded LNPs, and intralymphatic DC maturation was analysed by flow cytometry. C12-113/TLRa LNP significantly increased the percentage of matured DCs compared with C12-113 LNP (Fig. 4d,e and Supplementary Fig. 16). Next, iLNs and serum cytokines (TNF- α , IL-12p70 and IL-1 β) were analysed by ELISA at 6 and 24 h post-vaccination. While

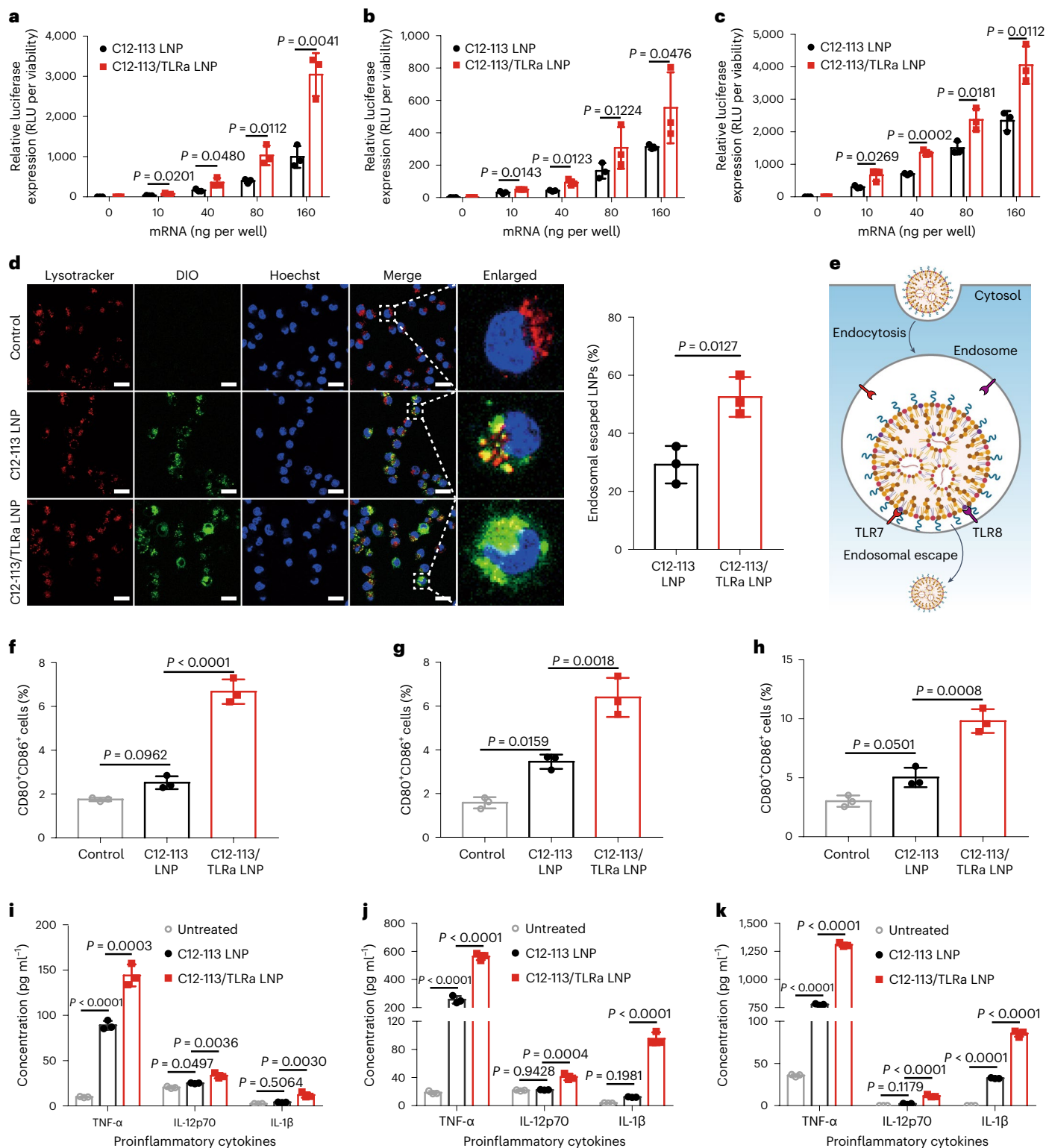


Fig. 3 | Adjuvant lipidoid-substituted LNP-mediated in vitro mRNA delivery and DC activation. **a–c**, Dose-dependent mRNA delivery ($n = 3$): DC2.4 cells (**a**), BMDCs (**b**) and MoDCs (**c**) were treated with mRNA-loaded C12-113 LNP or C12-113/TLRa LNP for 24 h. Results were normalized to untreated cells (0 ng mRNA per well). **d**, Representative confocal images of cellular uptake and quantification of LNP endosomal escape from three independent experiments. DC2.4 cells were treated with DiO-labelled LNPs for 2 h before staining with LysoTracker Deep Red and Hoechst 33342. The percentage of LNPs that escape endosomes was evaluated by computing the ratio of green signal in the Merge image (LNPs that escape endosomes) and DIO image (internalized LNPs) using ImageJ software ($n = 3$). Scale bars, 20 μm . **e**, A scheme illustrating the proposed mechanism

of enhanced endosomal escape by C12-113/TLRa LNP. The agonist–receptor interaction between C12-TLRa and TLR7/8 enhances LNP-mediated endosomal escape and DC maturation. **f–h**, Flow cytometry analysis of DC maturation ($n = 3$): DC2.4 cells (**f**), BMDCs (**g**) and MoDCs (**h**) were treated with SARS-CoV-2 mRNA-loaded LNPs (500 ng ml⁻¹) for 24 h and then stained with DC maturation markers CD80 and CD86. **i–k**, ELISA analysis of proinflammatory cytokines (TNF- α , IL-12p70 and IL-1 β , $n = 3$): DC2.4 cells (**i**), BMDCs (**j**) and MoDCs (**k**) were treated with SARS-CoV-2 mRNA-loaded LNPs (500 ng ml⁻¹) for 24 h before ELISA of cytokine production. Data are presented as mean \pm s.d. **a–d**, two-sided t -test; **f–k**, one-way ANOVA with Tukey's correction. Source data are provided as a Source Data file.

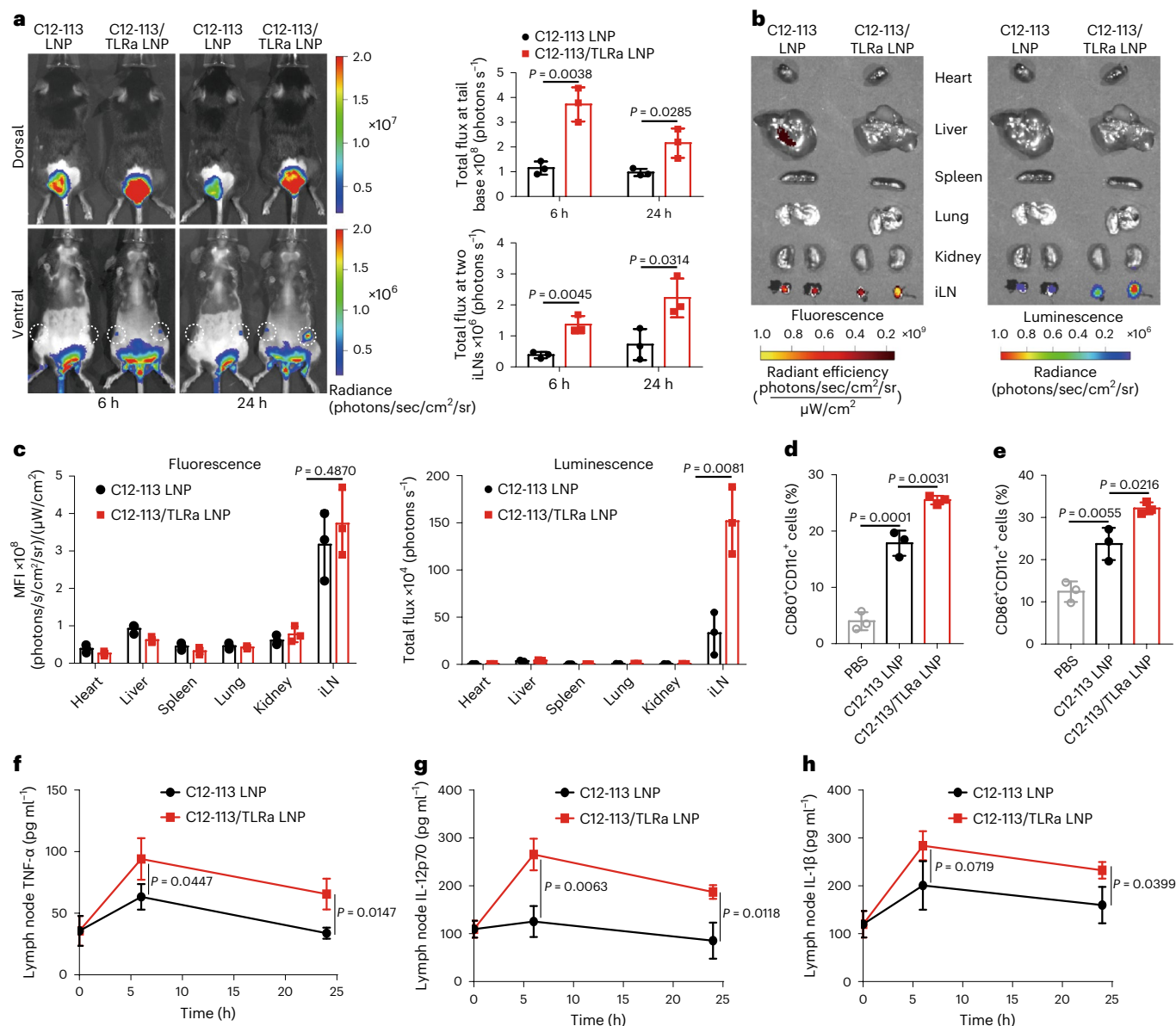


Fig. 4 | Adjuvant lipidoid-substituted LNP-mediated in vivo mRNA delivery and innate immune responses. **a**, In vivo bioluminescence imaging at 6 and 24 h post-treatment of mLuc-loaded LNPs ($n = 3$). Mice were s.c. injected with mLuc-loaded LNPs (5 μg mRNA per mouse) at the tail base. Total flux at the injection site and two iLNs were quantified. The dashed circles indicate iLNs. **b**, Ex vivo fluorescence and luminescence imaging. Mice were s.c. injected with DiR-labelled, mLuc-loaded LNPs (5 μg mRNA per mouse) at the tail base 24 h before they were sacrificed. Major organs and iLNs were collected for ex vivo imaging. **c**, Quantification of fluorescence and luminescence signals in **b** ($n = 3$). **d**, **e**, Flow cytometry analysis of matured DCs in iLNs ($n = 3$): CD80⁺CD11c⁺ cells

(**d**) and CD86⁺CD11c⁺ cells (**e**). At 24 h post-injection of SARS-CoV-2 mRNA-loaded LNPs, two iLNs from each mouse were harvested and processed to generate single-cell suspensions that were stained with CD11c, CD80 and CD86. **f–h**, ELISA analysis of intranodal proinflammatory cytokine production ($n = 3$). Two iLNs from each mouse were harvested at 6 or 24 h post-injection of SARS-CoV-2 mRNA-loaded LNPs and processed to generate a single-cell suspension that was cultured for 8 h before the supernatant was collected for ELISA analysis of TNF- α (**f**), IL-12p70 (**g**) and IL-1 β (**h**). Data are presented as mean \pm s.d. **a**, **c**, **f–h**, two-sided t -test; **d**, **e**, one-way ANOVA with Tukey's correction. Source data are provided as a Source Data file.

C12-113 LNP moderately and transiently induced intralymphatic cytokine production, C12-113/TLRa LNP elicited higher-magnitude and more persistent cytokine responses (Fig. 4f–h). As expected, due to the minimal systemic exposure of LNPs (Fig. 4b,c), these serum cytokine levels did not increase for either LNP (Supplementary Fig. 17). To further assess and compare the tolerability of these two mRNA-LNP vaccines, we evaluated the serum levels of acute phase protein, haptoglobin, and two inflammatory chemokines, interferon- γ -induced protein 10 (IP-10) and monocyte chemoattractant protein 1 (MCP-1), which have been demonstrated to be sensitive to s.c. injected mRNA-LNPs³⁹. Both LNPs induced transient and

comparable elevations of haptoglobin, IP-10 and MCP-1 levels (Supplementary Fig. 18). These results demonstrate that C12-113/TLRa substitution can greatly enhance the magnitude and duration of local innate immune responses without exacerbating systemic inflammation triggered by the pristine SARS-CoV-2 mRNA-LNP vaccine.

Adjuvant lipidoid substitution enhances cellular responses

We further investigated the adaptive immune responses elicited by original and adjuvant lipidoid-substituted SARS-CoV-2 mRNA-LNP vaccines. Mice were vaccinated twice, 3 weeks apart, using a prime-boost

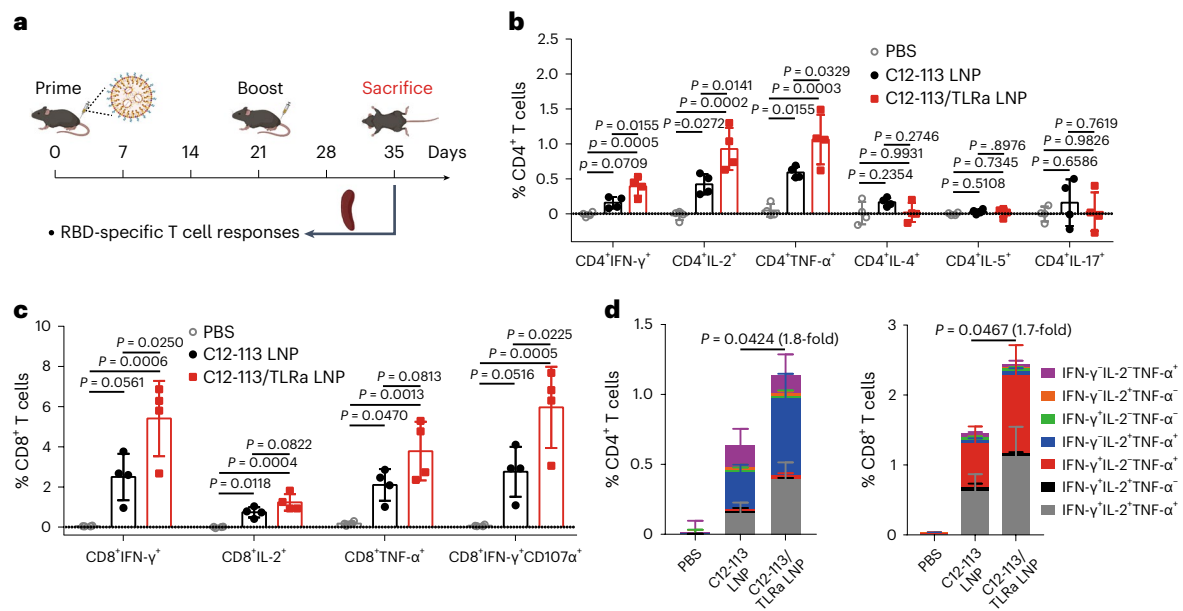


Fig. 5 | Cellular immune responses induced by adjuvant lipidoid-substituted SARS-CoV-2 mRNA-LNP vaccine. a, A scheme of the prime and boost vaccination strategy and analysis of the T cell responses. C57BL/6J mice were s.c. immunized twice with 5 μ g of C12-113 mRNA-LNP or C12-113/TLRa mRNA-LNP vaccine on days 0 and 21. **b, c**, Flow cytometry analysis of RBD-specific CD4⁺ (**b**) and CD8⁺ (**c**) T cell responses ($n = 4$). On day 35, spleens were harvested and processed to generate

single-cell suspensions that were stimulated with SARS-CoV-2 RBD peptide pools. T cells were stained for cytolytic marker CD107 α , Th1 (IFN- γ , IL-2 and TNF- α), Th2 (IL-4, IL-5) and Th17 (IL-17a) intracellular cytokine expression. **d**, Polyfunctional CD4⁺ (left) and CD8⁺ (right) T cells ($n = 4$). Data are presented as mean \pm s.d. **b–d**, One-way ANOVA with Tukey's correction. Source data are provided as a Source Data file.

strategy (Fig. 5a). Of note, neither skin abnormalities at the injection sites (Supplementary Fig. 19) nor body weight loss was observed after immunization (Supplementary Fig. 20). Two weeks after the boost dose, spleens from immunized mice were collected, and splenocytes were stimulated with SARS-CoV-2 receptor binding domain (RBD) peptide pools. Antigen-specific CD4⁺ and CD8⁺ T cells were measured by flow cytometry (Fig. 5b,c and Supplementary Fig. 21). Both LNPs elicited RBD-specific CD4⁺ T cells expressing Th1 cytokines (interferon (IFN)- γ , IL-2 and TNF- α); however, the effect elicited by C12-113/TLRa LNP was significantly higher than that elicited by C12-113 LNP (Fig. 5b). Moreover, neither vaccine formulation induced CD4⁺ T cells expressing type 2 (Th2) cytokines (IL-4, IL-5 and IL-17), supporting a Th1-biased T cell immune response. C12-113/TLRa LNP also elicited more RBD-specific CD8⁺ T cells expressing Th1 immune response cytokines (IFN- γ , IL-2 and TNF- α) and cytotoxic marker (CD107 α) (Fig. 5c). These results suggest that C12-113/TLRa-substituted SARS-CoV-2 mRNA-LNP vaccines can induce stronger RBD-specific Th1 and CD8⁺ T cell immune responses.

Polyfunctional T cells are generally considered immune correlates for protection against pathogens^{40–42}. Next we examined the polyfunctionality of these RBD-specific T cell responses. C12-113/TLRa LNP induced a significantly higher proportion of double- and triple-positive CD4⁺ and CD8⁺ T cells compared with the C12-113 LNP (Fig. 5d). The pattern of cytokine secretion of the double-positive cells was different between CD4⁺ (IL-2⁺ TNF- α ⁺) and CD8⁺ (IFN- γ ⁺ TNF- α ⁺) cells and consistent with the role of the helper and cytotoxic activities of these two different lymphocyte populations.

Adjuvant lipidoid substitution enhances humoral responses

Next, SARS-CoV-2 mRNA-LNP vaccine-induced humoral immune responses were analysed (Fig. 6a). Serum from vaccinated mice was subjected to endpoint dilution ELISA to determine the total RBD-specific IgG titres. Both mRNA-LNP vaccines triggered high levels of RBD-specific IgG (Fig. 6b); however, the IgG titre for C12-113/TLRa LNP was almost one order of magnitude higher than that for

C12-113 LNP (1.22×10^7 versus 1.35×10^6). Moreover, the ELISA analysis of RBD-specific IgG isotypes showed that C12-113/TLRa LNP elicited similar IgG1 titre and higher IgG2c titre with a higher IgG2c/IgG1 ratio compared with C12-113 LNP (Supplementary Fig. 22), further highlighting that adjuvant lipidoid-substituted LNPs tend to trigger stronger Th1-biased immune responses. Next, NAb levels were measured using a vesicular stomatitis virus (VSV)-based pseudovirus neutralization assay (Fig. 6c). While both mRNA-LNP vaccines induced high levels of NAbs against multiple SARS-CoV-2 pseudovirus variants, including D614G-mutated ancestor strain, Beta (B.1.351) variant and Delta (B.1.617.2) variant, C12-113/TLRa LNP elicited more NAbs against all three pseudoviruses as demonstrated by the higher 50% foci reduction neutralization titres (FRNT₅₀).

To investigate the induction of B cell memory, we assessed splenic B cell responses using fluorescent RBD probes (Supplementary Fig. 23)^{14,43}. C12-113/TLRa LNP vaccination significantly increased the number of RBD-specific B cells compared with C12-113 LNP (Fig. 6d), and these cells displayed a memory phenotype (CD38⁺GL7⁺; Fig. 6e). The majority of RBD-specific B cells in C12-113/TLRa LNP-vaccinated mice co-expressed the memory markers PD-L2 and CD80 (Fig. 6e), consistent with a potential for rapid differentiation into antibody-secreting cells (ASCs) upon rechallenge⁴⁴. Thus, C12-113/TLRa LNP vaccination generates a larger but phenotypically similar RBD-specific memory B cell pool.

Finally, we analysed bone marrow-resident long-lived plasma cells (LLPCs) 3 months after the second vaccination, which can mediate durable protection from infection by persistently producing antigen-specific antibodies. Bone marrow from immunized mice was collected, and various subsets of RBD-specific ASCs were characterized by enzyme-linked immunospot assay (ELISPOT). Whereas C12-113 LNP modestly induced the generation of RBD-specific IgG1-, IgG2a- and IgG2b-expressing ASCs (Fig. 6f–h), C12-113/TLRa LNP induced 6.7-, 2.4- and 6.5-fold more IgG1-, IgG2a- and IgG2b-expressing ASCs, respectively. Altogether, these results suggest that adjuvant lipidoid-substituted mRNA-LNP vaccine elicits stronger humoral immune responses and LLPC responses.

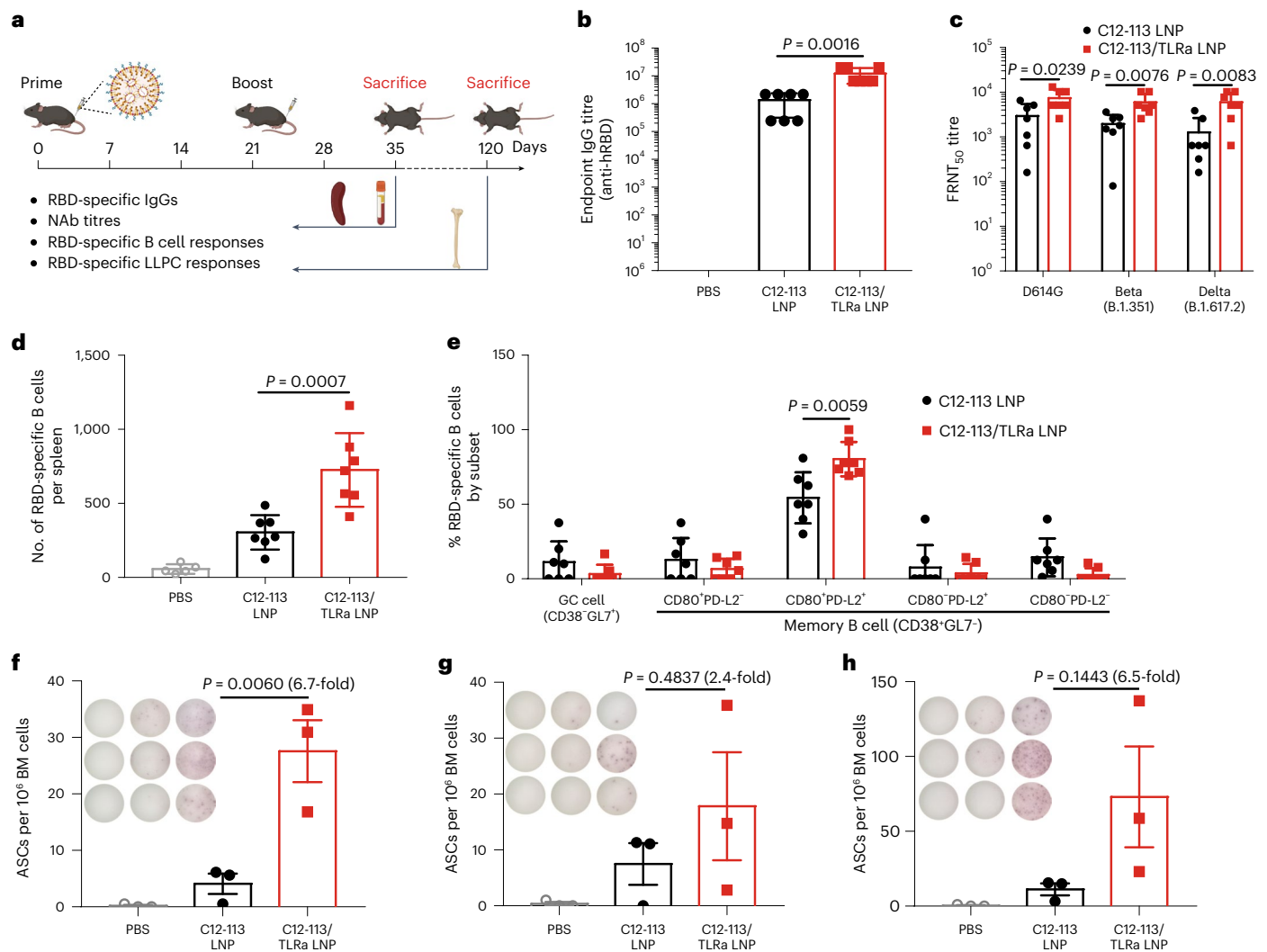


Fig. 6 | Humoral immune responses induced by adjuvant lipidoid-substituted SARS-CoV-2 mRNA-LNP vaccine. **a**, A scheme of the prime and boost vaccination strategy and analysis of the humoral immune responses. C57BL/6j mice were s.c. immunized twice with 5 μ g of C12-113 mRNA-LNP or C12-113/TLRa mRNA-LNP vaccine on days 0 and 21. **b**, RBD-specific IgG titre ($n = 7$). Serum was collected from vaccinated mice on day 35 and RBD-specific IgG levels were determined by endpoint dilution ELISA. **c**, NAb titre ($n = 7$). Serum was collected from vaccinated mice on day 35 and NAb levels were measured by a VSV-based pseudovirus neutralization assay. **d**, Number of RBD-specific B cells per spleen ($n = 5$ for PBS; $n = 7$ for the others). On day 35, spleens were harvested and processed to

generate single-cell suspensions that were stimulated with SARS-CoV-2 RBD peptide pools. Isotype-switched (IgD⁺IgM⁻) RBD-specific B cells were analysed by flow cytometry. **e**, Percentage of RBD-specific B cells by germinal centre (GC) or memory phenotype ($n = 7$). GC B cells were defined as CD38⁺GL7⁺. Memory B cells were defined as CD38⁺GL7⁻ and subsetted by PD-L2 and CD80 expression. **f–h**, Quantification at day 120 of RBD-specific IgG1 (**f**), IgG2b (**g**) and IgG2c (**h**) ASCs in bone marrow (BM) by ELISpot ($n = 3$). Insets: images of each well. Data are presented as mean \pm s.d. **b, d, f–h**, One-way ANOVA with Tukey's correction; **c, e**, two-sided *t*-test. Source data are provided as a Source Data file.

Enhanced immunogenicity of clinically relevant mRNA vaccines

To verify if adjuvant lipidoid substitution is a generally applicable strategy to enhance the adaptive immune responses of mRNA-LNP vaccines, we further chose the approved SM-102 LNP formulation for investigation (Supplementary Table 1). In a pilot study, we noticed that SM-102/TLRa LNP achieved greater mRNA transfection than SM-102 LNP after local injection as well, and both of them significantly outperformed C12-113 LNP or C12-113/TLRa LNP (Supplementary Fig. 24). To avoid the excessive expression of antigen, mice were vaccinated twice with SM-102 LNP or SM-102/TLRa LNP at a lower dose that achieved comparable protein expression as that in the previous study (Extended Data Fig. 1a and Supplementary Fig. 24). No skin abnormalities or body weight loss was observed during the experiment (Supplementary Figs. 25 and 26). Flow cytometry analysis of splenocytes from immunized

mice showed that SM-102/TLRa LNP elicited a significantly larger fraction of RBD-specific CD4⁺ and CD8⁺ T cells expressing Th1 cytokines (IFN- γ , IL-2 and TNF- α) compared with SM-102 LNP (Extended Data Fig. 1b,c and Supplementary Fig. 27). Moreover, more RBD-specific cytotoxic CD8⁺ T cells were induced by SM-102/TLRa LNP (Extended Data Fig. 1c). Further examination of these RBD-specific T cells showed that SM-102/TLRa LNP elicited a much higher proportion of double- and triple-positive CD4⁺ and CD8⁺ T cells in comparison with SM-102 LNP (Extended Data Fig. 1d). Together, these results suggest that C12-TLRa substitution can enhance the Th1-skewed, antigen-specific T cell immune responses of clinically relevant mRNA-LNP vaccines.

Next, humoral immune responses in immunized mice were studied (Extended Data Fig. 2a). SM-102/TLRa LNP achieved 5.4-fold higher anti-RBD IgG titre than SM-102 LNP (2.33×10^6 versus 4.30×10^5 ; Extended Data Fig. 2b). Moreover, SM-102/TLRa LNP-vaccinated

mice generated more NABs against all three SARS-CoV-2 pseudoviruses (D614G-mutated ancestor strain, Beta variant and Delta variant; Extended Data Fig. 2c). Flow cytometry analysis of splenocytes showed that SM-102/TLRa LNP elicited more RBD-specific B cells than SM-102 LNP, and these cells typically exhibited a memory phenotype (CD38⁺GL7⁺; Extended Data Fig. 2d,e). Moreover, most RBD-specific B cells in SM-102/TLRa LNP-vaccinated mice were PD-L2 and CD80 double positive, and the proportion of these cells was larger than that in SM-102 LNP-vaccinated mice (Extended Data Fig. 2e). These results demonstrate that C12-TLRa substitution can increase antigen-specific antibody responses and B cell responses of clinically relevant mRNA-LNP vaccines.

Together, all the above results confirm that adjuvant lipidoid substitution can enhance the immunogenicity of clinically relevant SARS-CoV-2 mRNA-LNP vaccines, which holds translational potential.

Conclusions

We developed a type of ionizable lipidoid—an adjuvant lipidoid—which serves not only as a structural component of LNPs to enhance mRNA delivery, but also as a functional moiety to increase the adjuvanticity of the LNPs. Adjuvant lipidoid-substituted SARS-CoV-2 mRNA-LNP vaccine significantly enhanced intralymphatic DC activation and intranodal pro-inflammatory cytokine production with good tolerability in mice due to its exclusive distribution and transfection at the injection site and draining lymph nodes. Due to the improved innate immunity, a more potent adaptive immunity against SARS-CoV-2 was established after immunization with adjuvant lipidoid-substituted mRNA-LNP vaccine, including strong Th1-biased cellular immune responses, antibody responses, B cell responses and LLPC responses. Moreover, we confirmed that adjuvant lipidoid substitution could enhance the immunogenicity of clinically relevant mRNA-LNP vaccines. Our study provides a LNP formulation basis for introducing adjuvant lipidoid to improve the quality and magnitude of adaptive immune responses for mRNA vaccines.

Online content

Any methods, additional references, Nature Portfolio reporting summaries, source data, extended data, supplementary information, acknowledgements, peer review information; details of author contributions and competing interests; and statements of data and code availability are available at <https://doi.org/10.1038/s41565-023-01404-4>.

References

- Le, T. T. et al. Evolution of the COVID-19 vaccine development landscape. *Nat. Rev. Drug Discov.* **19**, 667–668 (2020).
- Lauring, A. S. et al. Clinical severity of, and effectiveness of mRNA vaccines against, COVID-19 from Omicron, Delta, and Alpha SARS-CoV-2 variants in the United States: prospective observational study. *BMJ* **376**, e069761 (2022).
- Pardi, N. et al. mRNA vaccines—a new era in vaccinology. *Nat. Rev. Drug Discov.* **17**, 261–279 (2018).
- Yang, R. et al. A core-shell structured COVID-19 mRNA vaccine with favorable biodistribution pattern and promising immunity. *Signal Transduct. Target Ther.* **6**, 213 (2021).
- Brenner, S., Jacob, F. & Meselson, M. An unstable intermediate carrying information from genes to ribosomes for protein synthesis. *Nature* **190**, 576–581 (1961).
- Buschmann, M. D. et al. Nanomaterial delivery systems for mRNA vaccines. *Vaccines (Basel)* **9**, 65 (2021).
- Mitchell, M. J. et al. Engineering precision nanoparticles for drug delivery. *Nat. Rev. Drug Discov.* **20**, 101–124 (2021).
- Han, X. et al. An ionizable lipid toolbox for RNA delivery. *Nat. Commun.* **12**, 7233 (2021).
- Han, X., Mitchell, M. J. & Nie, G. Nanomaterials for therapeutic RNA delivery. *Matter* **3**, 1948–1975 (2020).
- Kariko, K. et al. Incorporation of pseudouridine into mRNA yields superior nonimmunogenic vector with increased translational capacity and biological stability. *Mol. Ther.* **16**, 1833–1840 (2008).
- Kariko, K. et al. Suppression of RNA recognition by Toll-like receptors: the impact of nucleoside modification and the evolutionary origin of RNA. *Immunity* **23**, 165–175 (2005).
- Oberli, M. A. et al. Lipid nanoparticle assisted mRNA delivery for potent cancer immunotherapy. *Nano Lett.* **17**, 1326–1335 (2017).
- Sahin, U., Kariko, K. & Tureci, O. mRNA-based therapeutics—developing a new class of drugs. *Nat. Rev. Drug Discov.* **13**, 759–780 (2014).
- Alameh, M. G. et al. Lipid nanoparticles enhance the efficacy of mRNA and protein subunit vaccines by inducing robust T follicular helper cell and humoral responses. *Immunity* **54**, 2877–2892.e7 (2021).
- Swaminathan, G. et al. A novel lipid nanoparticle adjuvant significantly enhances B cell and T cell responses to sub-unit vaccine antigens. *Vaccine* **34**, 110–119 (2016).
- Swaminathan, G. et al. A tetravalent sub-unit dengue vaccine formulated with ionizable cationic lipid nanoparticle induces significant immune responses in rodents and non-human primates. *Sci. Rep.* **6**, 34215 (2016).
- Coffman, R. L., Sher, A. & Seder, R. A. Vaccine adjuvants: putting innate immunity to work. *Immunity* **33**, 492–503 (2010).
- Dubensky, T. W. Jr. & Reed, S. G. Adjuvants for cancer vaccines. *Semin. Immunol.* **22**, 155–161 (2010).
- Gerster, J. F. et al. Synthesis and structure–activity-relationships of 1H-imidazo[4,5-c]quinolines that induce interferon production. *J. Med. Chem.* **48**, 3481–3491 (2005).
- Auderset, F. et al. A TLR7/8 agonist-including DOEPC-based cationic liposome formulation mediates its adjuvanticity through the sustained recruitment of highly activated monocytes in a type I IFN-independent but NF- κ B-dependent manner. *Front. Immunol.* **11**, 580974 (2020).
- Wang, J. et al. Lipidation approaches potentiate adjuvant-pulsed immune surveillance: a design rationale for cancer nanovaccine. *Front. Bioeng. Biotechnol.* **8**, 787 (2020).
- Islam, M. A. et al. Adjuvant-pulsed mRNA vaccine nanoparticle for immunoprophylactic and therapeutic tumor suppression in mice. *Biomaterials* **266**, 120431 (2021).
- Wilson, D. S. et al. Antigens reversibly conjugated to a polymeric glyco-adjuvant induce protective humoral and cellular immunity. *Nat. Mater.* **18**, 175–185 (2019).
- Lynn, G. M. et al. In vivo characterization of the physicochemical properties of polymer-linked TLR agonists that enhance vaccine immunogenicity. *Nat. Biotechnol.* **33**, 1201–1210 (2015).
- Love, K. T. et al. Lipid-like materials for low-dose, in vivo gene silencing. *Proc. Natl Acad. Sci. USA* **107**, 1864–1869 (2010).
- Zhang, Z. et al. Structural analysis reveals that Toll-like receptor 7 is a dual receptor for guanosine and single-stranded RNA. *Immunity* **45**, 737–748 (2016).
- Genile, F. et al. Structure based modeling of small molecules binding TLR7 by atomistic level simulations. *Molecules* **20**, 8316–8340 (2015).
- Shukla, N. M. et al. Potent adjuvanticity of a pure TLR7-agonistic imidazoquinoline dendrimer. *PLoS ONE* **7**, e43612 (2012).
- Rodell, C. B. et al. Development of adamantane-conjugated TLR7/8 agonists for supramolecular delivery and cancer immunotherapy. *Theranostics* **9**, 8426–8436 (2019).
- Billingsley, M. M. et al. Ionizable lipid nanoparticle-mediated mRNA delivery for human CAR T cell engineering. *Nano Lett.* **20**, 1578–1589 (2020).

31. Kauffman, K. J. et al. Optimization of lipid nanoparticle formulations for mRNA delivery in vivo with fractional factorial and definitive screening designs. *Nano Lett.* **15**, 7300–7306 (2015).
32. Li, B. et al. An orthogonal array optimization of lipid-like nanoparticles for mRNA delivery in vivo. *Nano Lett.* **15**, 8099–8107 (2015).
33. Riley, R. S. et al. Ionizable lipid nanoparticles for in utero mRNA delivery. *Sci. Adv.* **7**, eaba1028 (2021).
34. Whitehead, K. A. et al. Degradable lipid nanoparticles with predictable in vivo siRNA delivery activity. *Nat. Commun.* **5**, 4277 (2014).
35. Jayaraman, M. et al. Maximizing the potency of siRNA lipid nanoparticles for hepatic gene silencing in vivo. *Angew. Chem.* **124**, 8657–8661 (2012).
36. Laczko, D. et al. A single immunization with nucleoside-modified mRNA vaccines elicits strong cellular and humoral immune responses against SARS-CoV-2 in mice. *Immunity* **53**, 724–732.e7 (2020).
37. Alishetty, S. et al. Novel lipid nanoparticle provides potent SARS-CoV-2 mRNA vaccine at low dose with low local reactogenicity, high thermostability and limited systemic biodistribution. Preprint available at *Research Square* <https://doi.org/10.21203/rs.3.rs-798453/v1> (2021).
38. Pardi, N. et al. Expression kinetics of nucleoside-modified mRNA delivered in lipid nanoparticles to mice by various routes. *J. Control. Release* **217**, 345–351 (2015).
39. Davies, N. et al. Functionalized lipid nanoparticles for subcutaneous administration of mRNA to achieve systemic exposures of a therapeutic protein. *Mol. Ther. Nucleic Acids* **24**, 369–384 (2021).
40. Darrah, P. A. et al. Multifunctional TH1 cells define a correlate of vaccine-mediated protection against *Leishmania major*. *Nat. Med.* **13**, 843–850 (2007).
41. Precopio, M. L. et al. Immunization with vaccinia virus induces polyfunctional and phenotypically distinctive CD8⁺ T cell responses. *J. Exp. Med.* **204**, 1405–1416 (2007).
42. Almeida, J. R. et al. Superior control of HIV-1 replication by CD8⁺ T cells is reflected by their avidity, polyfunctionality, and clonal turnover. *J. Exp. Med.* **204**, 2473–2485 (2007).
43. Guerrini, G. et al. Characterization of nanoparticles-based vaccines for COVID-19. *Nat. Nanotechnol.* **17**, 570–576 (2022).
44. Zuccarino-Catania, G. V. et al. CD80 and PD-L2 define functionally distinct memory B cell subsets that are independent of antibody isotype. *Nat. Immunol.* **15**, 631–637 (2014).

Publisher's note Springer Nature remains neutral with regard to jurisdictional claims in published maps and institutional affiliations.

Springer Nature or its licensor (e.g. a society or other partner) holds exclusive rights to this article under a publishing agreement with the author(s) or other rightsholder(s); author self-archiving of the accepted manuscript version of this article is solely governed by the terms of such publishing agreement and applicable law.

© The Author(s), under exclusive licence to Springer Nature Limited 2023

¹Department of Bioengineering, University of Pennsylvania, Philadelphia, PA, USA. ²Department of Medicine, University of Pennsylvania, Philadelphia, PA, USA. ³Penn Institute for RNA Innovation, Perelman School of Medicine, University of Pennsylvania, Philadelphia, PA, USA. ⁴Department of Bioengineering, George Mason University, Fairfax, VA, USA. ⁵Intercollegiate Faculty of Biotechnology, University of Gdańsk & Medical University of Gdańsk, Gdańsk, Poland. ⁶Department of Pathology, University of Pennsylvania, Philadelphia, PA, USA. ⁷Department of Microbiology, University of Pennsylvania, Philadelphia, PA, USA. ⁸Department of Chemical Engineering, Polytechnique Montreal, Montreal, Quebec, Canada. ⁹Department of Chemistry, Case Western Reserve University, Cleveland, OH, USA. ¹⁰CAS Key Laboratory for Biomedical Effects of Nanomaterials and Nanosafety, CAS Center for Excellence in Nanoscience, National Center for Nanoscience and Technology, Beijing, People's Republic of China. ¹¹State Key Laboratory of Natural and Biomimetic Drugs, School of Pharmaceutical Sciences, Peking University, Beijing, People's Republic of China. ¹²Abramson Cancer Center, Perelman School of Medicine, University of Pennsylvania, Philadelphia, PA, USA. ¹³Institute for Immunology, Perelman School of Medicine, University of Pennsylvania, Philadelphia, PA, USA. ¹⁴Cardiovascular Institute, Perelman School of Medicine, University of Pennsylvania, Philadelphia, PA, USA. ¹⁵Institute for Regenerative Medicine, Perelman School of Medicine, University of Pennsylvania, Philadelphia, PA, USA. ¹⁶These authors contributed equally: Xuexiang Han, Mohamad-Gabriel Alameh. ✉e-mail: dreww@upenn.edu; mjmitch@seas.upenn.edu

Methods

Materials

TLR7/8 agonist 1 dihydrochloride was purchased from Cayman Chemical. 1,2-Epoxydodecane (C12) was obtained from Sigma-Aldrich. Core 200 was customized from Enamine, and other polyamine cores were purchased from Sigma-Aldrich and TCI. Anti-mouse CD16/32 antibody, APC anti-mouse CD11c antibody, FITC anti-mouse CD80 antibody, PE anti-mouse CD86 antibody, APC anti-human CD11c antibody, FITC anti-human CD80 antibody and PE anti-human CD86 antibody were purchased from Biolegend. Mouse IL-1 β uncoated ELISA, mouse IL-12p70 uncoated ELISA, mouse TNF- α uncoated ELISA, mouse MCP-1 uncoated ELISA, human IL-1 β uncoated ELISA, human IL-12p70 uncoated ELISA, human TNF- α uncoated ELISA, LysoTracker Deep Red, LysoTracker Green, DiO and DiR were bought from Invitrogen. Mouse haptoglobin ELISA and mouse IP-10 ELISA were obtained from Abcam. 1,2-Dioleoyl-*sn*-glycero-3-phosphoethanolamine, 1,2-distearoyl-*sn*-glycero-3-phosphocholine, DMG-PEG and cholesterol were obtained from Avanti Polar Lipids. DLin-MC3-DMA and SM-102 were purchased from MedChem Express. Codon-optimized m1 ψ -modified luciferase mRNA and SARS-CoV-2 diproline-modified spike (S2P) mRNA were produced by *in vitro* transcription¹⁴. Cy5-tagged luciferase mRNA was produced in house by incorporating Cy5-UTP (TriLink) into the *in vitro* transcription reaction.

Synthesis of adjuvant lipidoid

Adjuvant lipidoid C12-TLRa was synthesized by reacting epoxydodecane (C12) with TLR7/8 agonist 1 dihydrochloride using the ring-opening reaction²⁵. Briefly, 10 mg of TLR7/8 agonist 1 dihydrochloride was dissolved in 0.8 ml of ethanol in a glass vial with a magnetic stir bar. Then, 8 μ l of triethylamine was added to neutralize the hydrochloride before adding 20 mg of C12. The vial was sealed, and the mixture was stirred for 48 h at 80 °C. The crude product was purified by a CombiFlash NextGen 300+ chromatography system (Teledyne ISCO) with gradient elution from CH₂Cl₂ to 75:22:3 CH₂Cl₂/MeOH/NH₄OH (aq.). The desired fraction was collected (yield, 44%). C12-TLRa was characterized by mass spectrometry (calculated MS, 728.12; found [M + 2H]²⁺, 365.25) and NMR spectroscopy. ¹H NMR (400 MHz, DMSO-*d*₆) δ (ppm): 7.78 (d, *J* = 8.3 Hz, 1H), 7.57 (doublet of doublets, *J* = 8.4, 1.3 Hz, 1H), 7.35–7.29 (m, 1H), 7.27 (d, *J* = 7.9 Hz, 2H), 7.05–7.00 (m, 1H), 6.98 (d, *J* = 8.0 Hz, 2H), 5.84 (s, 2H), 3.61–3.47 (m, 2H), 3.44 (s, 2H), 2.90 (t, *J* = 7.7 Hz, 2H), 2.68 (q, *J* = 1.9 Hz, 2H), 2.34 (t, *J* = 2.8 Hz, 2H), 1.69 (quintet, *J* = 7.6 Hz, 2H), 1.37 (doublet of triplets, *J* = 14.9, 7.5 Hz, 2H), 1.22 (s, 36H), 0.90–0.81 (m, 9H).

General method for the synthesis of polyamine-derived lipidoids

The polyamine cores were reacted with excess moles of C12 as needed to saturate the amines^{25,33}. Taking C12-113 as an example, 113 core (1 equiv.) was mixed with C12 (4.8 equiv.) for 48 h at 80 °C in a neat condition. The crude product was used for the initial library screening. To purify the top-performing C12-113 lipidoid, the crude product was separated as described above, and the fully saturated product was collected and identified by mass spectrometry (calculated MS, 854.49; found [M + 2H]²⁺, 429.13) and used for subsequent experiments.

Structural simulation of agonist–TLR7 interaction

The structures of TLR7/8 agonist 1 and C12-TLRa were first optimized by molecular dynamics simulation with the CHARMM force field⁴⁵. The exact TLR7 protein crystal structure was derived from the structure of the TLR7/R848 complex (PDB ID, 5GMH), removing any ligands or solvent molecules²⁶. Structural simulation between TLR7 dimer and agonists was carried out by CDocker docking simulation⁴⁶ and *in situ* structural superimposition. Potential non-covalent interactions, binding pockets and overviews of the binding sites between TLR7 dimer and the corresponding agonists were generated using BIOVIA Discovery Studio 2018.

LNP formulation

LNPs were formulated by microfluidic mixing³⁰. Briefly, an ethanol phase containing lipidoid (with or without C12-TLRa substitution), phospholipid, cholesterol and DMG-PEG at a designated molar ratio (Supplementary Table 1) was mixed with an aqueous phase (10 mM citrate buffer, pH 3) containing mRNA at a flow rate ratio of 1:3 and at a lipidoid/RNA weight ratio of 10:1 in a microfluidic chip device. LNPs were dialysed against 1 \times PBS in a 20 kDa molecular weight cut-off cassette for 2 h, sterilized through a 0.22 μ m filter and stored at 4 °C. DiO- or DiR-labelled LNPs were obtained by mixing DiO or DiR (1 mol% of total lipids) with LNPs before dialysis.

LNP characterization

The hydrodynamic size, PDI and zeta potential of LNPs were measured using a Zetasizer Nano ZS90 (Malvern Instruments). The morphology of LNPs was characterized by TEM (JEOL 1010) and cryo-EM (Titan Krios, Thermo Fisher) with a K3 Bioquantum (Gatan). The mRNA encapsulation efficiency and the *pK_a* of LNPs were determined using a modified Quant-iT RiboGreen RNA assay (Invitrogen) and a 6-(*p*-toluidinyl)naphthalene-2-sulfonic acid assay, respectively^{30,33}. LNP formulations were routinely examined by the Limulus amoebocyte lysate (LAL) test, and endotoxin levels were consistently found to be <1 endotoxin unit per ml.

Cell culture and animal studies

The HEK-Blue mTLR7 cell line was kindly provided by J. Shi at Harvard Medical School, who obtained it from InvivoGen (#hkb-mtlr7). These cells were maintained according to vendor's instruction. Murine macrophage DC2.4 cell line was obtained from American Type Culture Collection and maintained in Dulbecco's modified Eagle's medium (DMEM) supplemented with 10% foetal bovine serum, 100 U ml⁻¹ penicillin and 100 μ g ml⁻¹ streptomycin. All cells were cultured at 37 °C in a humidified incubator of 5% CO₂, and routinely tested for mycoplasma contamination.

BMDCs were generated from C57BL/6 mice. Briefly, bone marrow cells were flushed from mouse femurs and tibias, lysed by ammonium–chloride–potassium (ACK) buffer to remove red blood cells and then cultured in RPMI 1640 medium supplemented with 10% foetal bovine serum, 100 U ml⁻¹ penicillin and 100 μ g ml⁻¹ streptomycin, 1% HEPES, 0.1 mM β -mercaptoethanol, 20 ng ml⁻¹ murine IL-4 (#214-14, PeproTech) and 20 ng ml⁻¹ murine granulocyte-macrophage colony stimulating factor (#315-03, PeproTech). On day 6, non-adherent and loosely adherent cells were collected for studies.

MoDCs were generated from a 38-year-old healthy male volunteer donor. Monocytes were isolated from donated apheresis blood using the RosetteSep Human Monocyte Enrichment Cocktail (#15068, Stemcell Technologies), and provided by the Human Immunology Core at the University of Pennsylvania. These cells were induced into MoDCs by culturing in complete RPMI medium supplemented with 20 ng ml⁻¹ human IL-4 (#574002, Biolegend) and 20 ng ml⁻¹ human granulocyte-macrophage colony stimulating factor (#572902, Biolegend) for 6 days. This study was approved by the Institutional Review Board of the University of Pennsylvania (#705906). Informed consent was obtained from the donor, who was compensated for this blood donation.

All animal protocols were approved by the Institutional Animal Care and Use Committee of the University of Pennsylvania (#806540), and animal procedures were performed in accordance with the Guidelines for Care and Use of Laboratory Animals at the University of Pennsylvania. C57BL/6 female mice (6–8 weeks of age, 18–20 g body weight) were purchased from Jackson Laboratory.

In vitro mLuc delivery

DC cells, BMDCs or MoDCs were seeded onto a 96-well plate at a density of 10,000 per well overnight and then mLuc-loaded LNPs were used to treat cells at the indicated doses for 24 h. Luciferase expression was

evaluated by Luciferase Reporter 1000 Assay System (E4550, Promega), and cell viability was measured using a CellTiter-Glo Luminescent Cell Viability Assay (G7572, Promega) according to the manufacturer's protocols. The relative luciferase expression was reported as relative light units normalized to cell viability. Free mRNA was used as a control.

TLR7 reporter assay

The TLR7-agonistic activity of C12-TLRa was tested on HEK-Blue mTLR7 reporter cells using a HEK-Blue Detection Kit (#hb-det2, InvivoGen) according to the manufacturer's instructions. Briefly, HEK-Blue mTLR7 reporter cells were seeded into a 96-well plate at a density of 40,000 cells per well in HEK-Blue Detection medium containing different concentrations of C12-TLRa. After incubation for 24 h, the absorbance at 650 nm was measured using a plate reader (Infinite M200, Tecan) and data were normalized to untreated cells. TLR7/8 agonist 1 was used as a positive control. Similarly, the TLR7-agonistic activity of LNPs was measured.

Cellular uptake

DC2.4 cells were seeded into 35 mm glass-bottom dishes for 24 h and then treated with DiO-labelled C12-113 LNP or DiO-labelled C12-113/TLRa LNP at an mRNA concentration of 500 ng ml⁻¹ for 2 h. Cells were sequentially stained with LysoTracker Deep Red (100 nM) for 30 min and Hoechst 33342 (10 µg ml⁻¹) for 5 min. Images were taken immediately using a confocal laser scanning microscope (LSM 710, Zeiss).

Analysis of DC maturation and cytokine production in vitro

DC2.4 cells or BMDCs were seeded into a 12-well plate at a density of 1×10^6 cells per well overnight and then treated with SARS-CoV-2 mRNA-loaded LNPs (500 ng ml⁻¹) for 24 h. Cell cultures were collected for ELISA of TNF-α, IL-12p70 and IL-1β. Cells were collected, blocked with anti-mouse CD16/32 antibody and then stained with APC anti-mouse CD11c antibody, FITC anti-mouse CD80 antibody and PE anti-mouse CD86 antibody for 30 min at 4 °C before being analysed by flow cytometry (BD, LSR II). Similarly, MoDCs were treated. Cell cultures were collected for ELISA of human TNF-α, IL-12p70 and IL-1β. MoDCs were collected and stained with APC anti-human CD11c antibody, FITC anti-human CD80 antibody and PE anti-human CD86 antibody before analysis. Antibodies were used according the manufacturer's instruction with a typical dilution at 1:100.

Analysis of DC maturation and cytokine production in vivo

Two iLNs from each mouse were harvested at 24 h post-injection of SARS-CoV-2 mRNA-loaded LNPs (5 µg mRNA per mouse) at the tail base and were gently mechanically disrupted using sterile pestles in 0.1 ml of RPMI complete medium in a 1.5 ml tube. The resulting cell suspensions were collected, blocked with anti-mouse CD16/32 antibody and then stained with APC anti-mouse CD11c antibody, FITC anti-mouse-CD80 antibody and PE anti-mouse-CD86 antibody before being analysed by flow cytometry.

Blood was collected into serum separator tubes (BD #365967) through the retro-orbital route at 6 and 24 h post-immunization. Serum was separated from blood following an incubation period of 30 min at room temperature (r.t.), and samples were centrifuged at 10,000g for 5 min. The serum was stored at -20 °C until use. To analyse the intralymphatic cytokine production, the resulting cell suspensions from iLNs were placed to a 96-well plate at a density of 10,000 cells per 100 µl per well and cultured for 8 h. Supernatant was collected for ELISA of TNF-α, IL-12p70 and IL-1β together with serum samples. Additionally, serum at 6, 24 and 48 h post-immunization was collected for ELISA of haptoglobin, IP-10 and MCP-1.

Distribution and transfection of LNPs in vivo

Mice were s.c. injected at the tail base with mLuc-loaded LNPs at a dose of 5 µg mRNA per mouse. At 6 or 24 h post-injection, mice were intraperitoneally (i.p.) injected with D-luciferin potassium salt (150 mg

per kg (body weight)), and bioluminescence imaging was performed on an IVIS imaging system (PerkinElmer). To enable concurrent bioluminescence and fluorescence imaging, DiR-labelled, mLuc-loaded LNPs were s.c. injected into mice. At 24 h post-injection, mice were i.p. injected with D-luciferin potassium salt, and major organs and iLNs were collected for bioluminescence and fluorescence imaging.

In vivo immunization

Mice were s.c. immunized with SARS-CoV-2 mRNA-loaded LNPs at a dose of 1 or 5 µg mRNA per mouse twice using a prime-boost strategy at a 3 week interval. Body weight was recorded twice a week during the experiment. Serum was collected using serum separator tubes as described above, stored at -20 °C and used for ELISA and virus neutralization assay. Two weeks after the boost vaccination, mice were anaesthetized and spleens were collected for flow cytometry analysis.

Determination of anti-RBD antibody titres using ELISA

Purified SARS-CoV-2 His tagged RBD (1 µg ml⁻¹) (Sino Biological, #40592-V08H) was used to coat High Bind Stripwell Corning 96-well clear polystyrene microplates overnight. Plates were washed with wash buffer (0.05% Tween 20/PBS) once, and blocked for 2 h at r.t. using a solution of heat-inactivated, IgG-depleted, protease-free bovine serum albumin (2% w/v BSA/PBS). Afterwards, plates were washed three times, and mouse sera were serially diluted in the blocking solution and incubated for 2 h at r.t. Plates were washed three times before adding horseradish-peroxidase-conjugated anti-mouse secondary antibody specific to total IgG (1:10,000, Abcam #ab97040) or subclasses (IgG1, 1:10,000, Abcam, #ab98693; IgG2c, 10,000, Abcam, #ab98722) in blocking buffer. Plates were incubated for 1.5 h and washed three times before the addition of 100 µl KPL 3,3',5,5'-tetramethylbenzidine substrate per well for 8 min. The reaction was stopped by adding 50 µl of 2 N sulfuric acid, and the absorbance was measured at 450 nm using a SpectraMax 190 microplate reader. RBD-specific IgG endpoint dilution titre was defined as the highest dilution of serum to give an optical density greater than the cut-off optical density value determined using the Frey method⁴⁷.

Pseudovirus neutralization assay

A VSV pseudotype with SARS-CoV-2 S was first produced³⁶. We performed an antibody neutralization assay using VSVΔG-RFP SARS-CoV-2. Vero E6 cells stably expressing TMPRSS2 were seeded in 100 µl DMEM at 2.5×10^4 cells per well in a 96-well collagen-coated plate. After 12 h, twofold serially diluted serum samples were mixed with VSVΔG-RFP SARS-CoV-2 pseudotype virus (50–200 focus-forming units per well) encoding the spike of D614G, Beta or Delta variant and incubated for 1 h at 37 °C. A mouse anti-VSV Indiana G, 8G5F11 (#Ab01401-2.0, Absolute Antibody), was also included in this mixture to neutralize any potential VSV-G carryover virus at a concentration of 100 ng ml⁻¹. The antibody-virus mixture was then used to replace the media on Vero E6 TMPRSS2 cells. At 20 h post-infection, the cells were washed and fixed with 4% PFA before visualization on an S6 FluoroSpot Analyzer (CTL). Individual infected foci were enumerated, and the values were compared with control wells without antibody. The focus reduction neutralization titre 50% (FRNT₅₀) was measured as the greatest serum dilution at which focus count was reduced by at least 50% relative to control cells that were infected with pseudotype virus in the absence of mouse serum. FRNT₅₀ titres for each sample were measured in two technical replicates performed on separate days.

Flow cytometry analysis of T and B cells

T cell. Spleens were collected, processed as single cells, filtered using a 70 µm cell strainer in complete RPMI 1640 and centrifuged, and red blood cells lysed in ACK lysis buffer to obtain a clear single-cell suspension. To measure antigen-specific T cells, two million splenocytes were stimulated with 2.5 µg ml⁻¹ of SARS-CoV-2 RBD peptide pools

(#PM-WCPV-S-RBD-1, JPT) in a FACS tube for 6 h at 37 °C, 5% CO₂ with 2 mg ml⁻¹ anti-CD28 (Tonbo #40-0281-M001) providing co-stimulation. Stimulations proceeded for 1 h before adding 5 mg ml⁻¹ brefeldin A (Biolegend #420601), 2 mM monensin (Biolegend #420701) and 5 mg ml⁻¹ anti-CD107a Alexa Fluor 647 (Biolegend #121610) for 5 h. DMSO served as a negative control, and the combination of 50 mg ml⁻¹ phorbol 12-myristate 13-acetate and 1 mg ml⁻¹ ionomycin served as a positive control. After a total of 6 h, samples were washed with PBS, stained with Live/Dead Aqua for 5 min, blocked using anti-mouse CD16/32 antibody for 20 min and stained extracellularly for 30 min using antibodies (Supplementary Figs. 21d and 27d). Cells were washed in FACS buffer, fixed and permeabilized using the Cytofix/Cytoperm kit (BD Biosciences #554714), and stained intracellularly using antibodies for 30 min (Supplementary Figs. 21d and 27d). After intracellular staining, cells were washed twice and fixed with 300 µl (1% PFA), and samples were acquired on a BD LSR II equipped with four laser lines and 18 photomultiplier tubes. The gating strategy, and the antibody list and catalogue numbers are provided in Supplementary Figs. 21 and 27.

Memory B cell. Splens were collected, processed as single cells, filtered using a 40 µm cell strainer in complete RPMI 1640 and centrifuged at 300g for 5 min; red blood cells were lysed with ACK (1 min), washed twice and counted, and two million cells per sample were incubated with anti-mouse CD16/32 antibody for 20 min at 4 °C. Cells were then washed with FACS buffer (1% BSA/PBS) and stained for 1 h using antibodies (Supplementary Fig. 23d). Following staining, cells were washed twice and fixed with 300 µl (1% PFA), and samples were acquired on a BD LSR II equipped with four laser lines and 18 photomultiplier tubes. The gating strategy, and the antibody list, fluorescent RBD probes¹⁴ and catalogue numbers are provided in Supplementary Fig. 23.

ELISpot assay

Bone marrow was flushed from femurs and tibia into FACS buffer and filtered through a 63 µm Nitex mesh. Red blood cells were lysed in ACK buffer for 5 min on ice, and washed twice with FACS buffer. The resulting cells were counted using a Beckman Coulter ViCell. MultiScreenHTS IP filter plates, 0.45 µm (Millipore Sigma, MSIPS4W10), were coated with RBD protein antigen at 10 µg ml⁻¹ in sodium carbonate/sodium bicarbonate buffer pH 9.6 (35 mM NaHCO₃ and 15 mM Na₂CO₃) for 1 h at 37 °C. Plates were then washed with 200 µl PBS per well three times and blocked at 37 °C in complete RPMI for 30 min. Bone marrow cells were plated in six halving dilutions beginning with one million total bone marrow cells per well and incubated overnight in complete RPMI. Plates were then washed with wash buffer (1× PBS + 0.1% Tween 20) five times, and biotinylated anti-IgG detection antibody (goat anti-mouse IgG human ads-BIOT; Southern Biotech, 1030-08) was added at a final dilution of 3 µg ml⁻¹ in 2% BSA/PBS and incubated at r.t. for 1 h. Plates were once again washed five times, and streptavidin-alkaline phosphatase (1:20,000 dilution in 2% BSA/PBS) was added prior to incubation at r.t. for 30 min. Plates were then washed five times with wash buffer, and 50 µl per well 5-bromo-4-chloro-3-indolyl-phosphate/nitro blue tetrazolium chloride solution (Sigma, #B1911, 100 ml) was added for -10 min or until spots developed at which time the reaction was quenched with 100 µl 1 M sodium phosphate monobasic solution. After plates were rinsed with deionized H₂O and dried overnight, they were scanned and counted using an S6 FluoroSpot Analyzer.

Statistics and reproducibility

All data are presented as mean ± s.d. Student's *t*-test or one-way analysis of variance (ANOVA) followed by Tukey's test was applied for comparison between two groups or among multiple groups using Graphpad Prism 7.0, respectively. *P* < 0.05 was considered to be statistically significant. Each experiment is repeated at least three times independently with similar results, and the representative dataset is presented.

Reporting summary

Further information on research design is available in the Nature Portfolio Reporting Summary linked to this article.

Data availability

All data that support the findings of this study are provided within the paper and its Supplementary Information. The raw datasets generated during the study are provided within the source data. Source data are available for Figs. 2–6, Extended Data Figs. 1 and 2, and Supplementary Figs. 4, 6–8, 10–12, 15, 17, 18, 20, 22, 24 and 26. The crystal structure data of TLR7 are available in the Protein Data Bank (PDB) under PDB ID: 5GMH. Source data are provided with this paper.

References

- Momany, F. A. & Rone, R. Validation of the general-purpose Quanta(R)3.2/Charmm(R) force-field. *J. Comput. Chem.* **13**, 888–900 (1992).
- Wu, G. et al. Detailed analysis of grid-based molecular docking: a case study of CDOCKER—a CHARMm-based MD docking algorithm. *J. Comput. Chem.* **24**, 1549–1562 (2003).
- Frey, A., Di Canzio, J. & Zurakowski, D. A statistically defined endpoint titer determination method for immunoassays. *J. Immunol. Methods* **221**, 35–41 (1998).

Acknowledgements

M.J.M. acknowledges support from a US National Institutes of Health (NIH) Director's New Innovator Award (DP2 TR002776), a US National Science Foundation CAREER Award (CBET-2145491), an American Cancer Society Research Scholar Grant (RSG-22-122-01-ET) and a Burroughs Wellcome Fund Career Award at the Scientific Interface (CASI). K.B. acknowledges support from the Polish National Agency for Academic Exchange (number PNN/IWA/2019/00057, Poland). The authors thank S. Steimle from the Beckman Center for Cryo Electron Microscopy at the University of Pennsylvania for help in characterizing the morphology of LNPs. The authors acknowledge the Cell Center Services Facility at the University of Pennsylvania for assistance with the LAL test. The authors thank L. Chen, M. A. Eldabbas and E. Maddox of the Human Immunology Core at the University of Pennsylvania for providing human monocytes, who are supported by NIH P30 AIO45008 and P30 CA016520. Elements of Figs. 1, 3, 5 and 6 created with BioRender.com.

Author contributions

X.H., M.-G.A. and M.J.M. conceptualized, conceived and designed experiments. X.H., M.-G.A., K.B., J.J.K., K.L. and M.G. performed experiments. M.-G.A. and P.B. provided reagents and protocols. X.H., M.-G.A., J.J.K., N.G. and L.X. analysed data. X.H., M.-G.A., D.W. and M.J.M. wrote the manuscript. All authors discussed and edited the manuscript content.

Competing interests

X.H. and M.J.M. have filed a patent application based on this work. In accordance with the University of Pennsylvania policies and procedures and our ethical obligations as researchers, we report that D.W. is named on patents that describe the use of nucleoside-modified mRNA as a platform to deliver therapeutic proteins and vaccines. D.W. and M.G.A. are also named on patents describing the use of lipid nanoparticles, and lipid compositions for nucleic acid delivery and vaccination. We have disclosed those interests fully to the University of Pennsylvania, and we have in place an approved plan for managing any potential conflicts arising from licensing of our patents. The remaining authors declare no competing interests.

Additional information

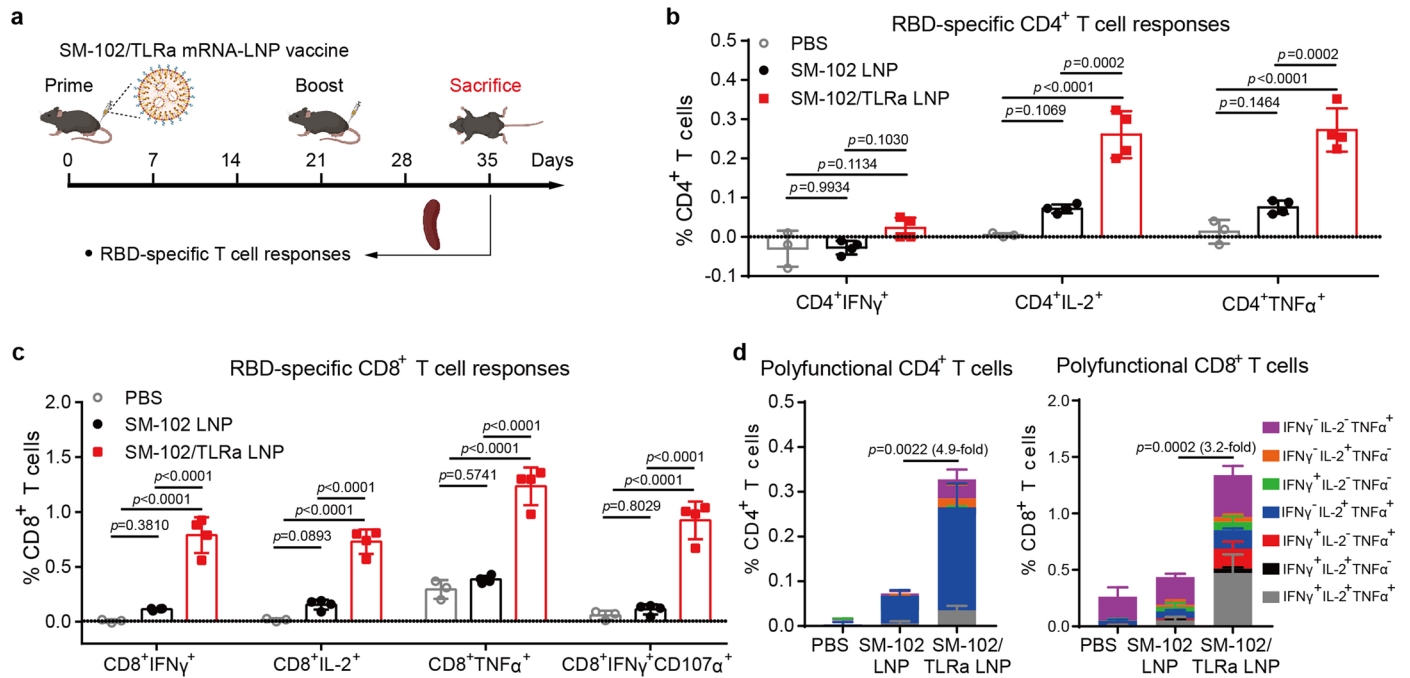
Extended data is available for this paper at <https://doi.org/10.1038/s41565-023-01404-4>.

Supplementary information The online version contains supplementary material available at <https://doi.org/10.1038/s41565-023-01404-4>.

Correspondence and requests for materials should be addressed to Drew Weissman or Michael J. Mitchell.

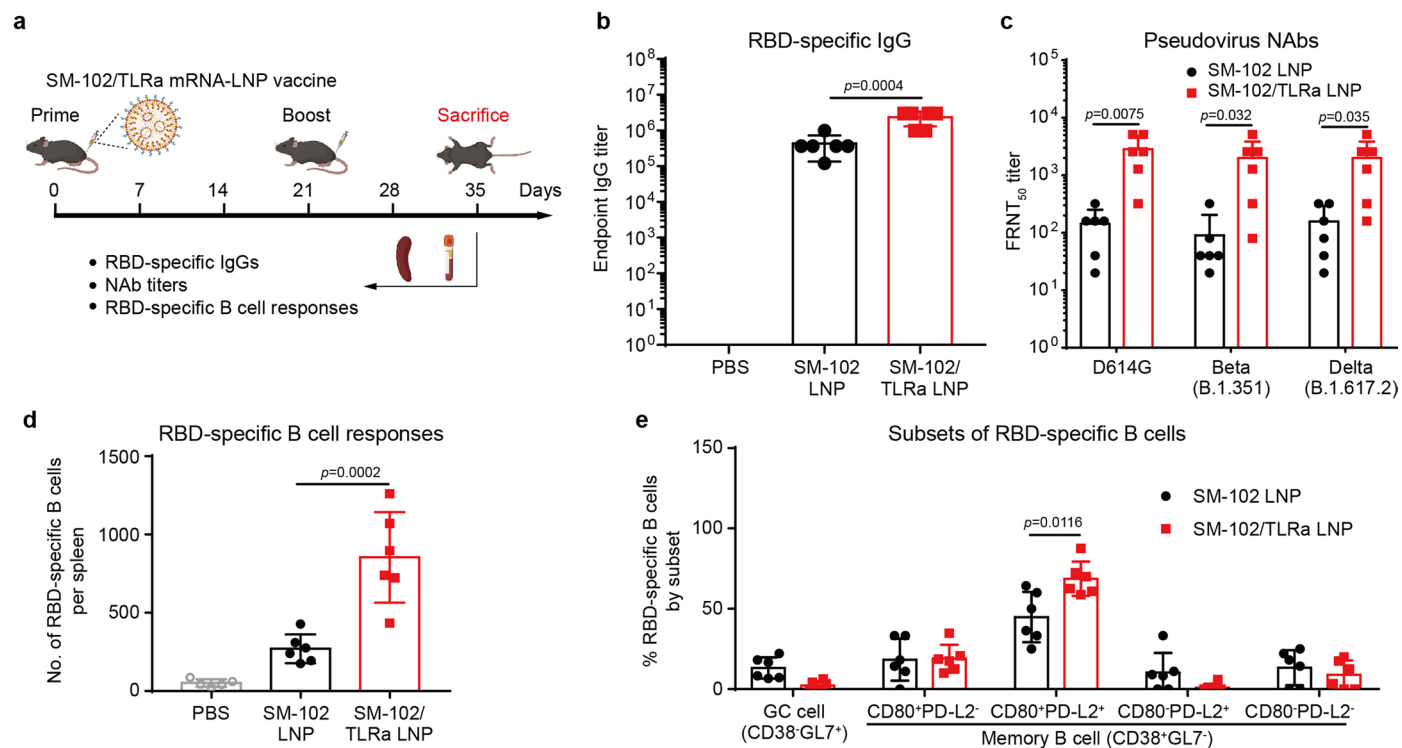
Peer review information *Nature Nanotechnology* thanks Francis Szoka, Anna Blakney and Donata Medaglini for their contribution to the peer review of this work.

Reprints and permissions information is available at www.nature.com/reprints.



Extended Data Fig. 1 | Cellular immune responses induced by adjuvant lipidoid-substituted clinically relevant SARS-CoV-2 mRNA vaccines. a, A scheme of the prime and boost vaccination strategy and the analysis of T cell responses. C57BL/6 J mice were s.c. immunized twice with 1 μ g of SM-102 mRNA-LNP or SM-102/TLRa mRNA-LNP vaccine on Day 0 and 21. **b, c**, Flow cytometry analysis of RBD-specific CD4⁺ and CD8⁺ T cell responses (n = 3 for PBS; n = 4 for

the others). On Day 35, spleens were harvested and processed to generate single cell suspensions that were stimulated with SARS-CoV-2 RBD peptide pools. T cells were stained for cytolytic marker CD107 α and Th1 (IFN- γ , IL-2 and TNF- α) intracellular cytokine expression. **d**, Polyfunctional CD4⁺ and CD8⁺ T cells (n = 3 for PBS; n = 4 for the others). Data are presented as mean \pm SD. **b–d** one-way ANOVA with Tukey’s correction. Source data are provided as a Source Data file.



Extended Data Fig. 2 | Humoral immune responses induced by adjuvant lipidoid-substituted clinically relevant SARS-CoV-2 mRNA vaccines.

a, A scheme of the prime and boost vaccination strategy and the analysis of humoral immune responses. C57BL/6 J mice were s.c. immunized twice with 1 μ g of SARS-CoV-2 mRNA-LNP vaccine on Day 0 and 21. **b**, RBD-specific IgG titre ($n = 5$ for PBS; $n = 6$ for the others). Serum was collected from vaccinated mice on Day 35 and RBD-specific IgG levels were determined by endpoint dilution ELISA. **c**, Neutralizing antibody (NAb) titre ($n = 6$). Serum was collected from vaccinated mice on Day 35 and NAb levels were measured by a VSV-based pseudovirus

neutralization assay. **d**, Number of RBD-specific B cells per spleen ($n = 5$ for PBS; $n = 6$ for the others). Spleens were harvested and processed to generate single cell suspensions that were stimulated with SARS-CoV-2 RBD peptide pools. Isotype-switched (IgD⁺IgM⁻) RBD-specific B cells were analysed by flow cytometry. **e**, Percentage of RBD-specific B cells by germinal center (GC) or memory phenotype ($n = 6$). GC B cells were defined as CD38⁻GL7⁺. Memory B cells were defined as CD38⁺GL7⁻ and subsetted by PD-L2 and CD80 expression. Data are presented as mean \pm SD. **b** and **d** one-way ANOVA with Tukey's correction. **c**, **e** two-sided *t*-test. Source data are provided as a Source Data file.

Reporting Summary

Nature Portfolio wishes to improve the reproducibility of the work that we publish. This form provides structure for consistency and transparency in reporting. For further information on Nature Portfolio policies, see our [Editorial Policies](#) and the [Editorial Policy Checklist](#).

Statistics

For all statistical analyses, confirm that the following items are present in the figure legend, table legend, main text, or Methods section.

n/a Confirmed

- | | | |
|-------------------------------------|-------------------------------------|--|
| <input type="checkbox"/> | <input checked="" type="checkbox"/> | The exact sample size (n) for each experimental group/condition, given as a discrete number and unit of measurement |
| <input type="checkbox"/> | <input checked="" type="checkbox"/> | A statement on whether measurements were taken from distinct samples or whether the same sample was measured repeatedly |
| <input type="checkbox"/> | <input checked="" type="checkbox"/> | The statistical test(s) used AND whether they are one- or two-sided
<i>Only common tests should be described solely by name; describe more complex techniques in the Methods section.</i> |
| <input checked="" type="checkbox"/> | <input type="checkbox"/> | A description of all covariates tested |
| <input type="checkbox"/> | <input checked="" type="checkbox"/> | A description of any assumptions or corrections, such as tests of normality and adjustment for multiple comparisons |
| <input type="checkbox"/> | <input checked="" type="checkbox"/> | A full description of the statistical parameters including central tendency (e.g. means) or other basic estimates (e.g. regression coefficient) AND variation (e.g. standard deviation) or associated estimates of uncertainty (e.g. confidence intervals) |
| <input type="checkbox"/> | <input checked="" type="checkbox"/> | For null hypothesis testing, the test statistic (e.g. F , t , r) with confidence intervals, effect sizes, degrees of freedom and P value noted
<i>Give P values as exact values whenever suitable.</i> |
| <input checked="" type="checkbox"/> | <input type="checkbox"/> | For Bayesian analysis, information on the choice of priors and Markov chain Monte Carlo settings |
| <input checked="" type="checkbox"/> | <input type="checkbox"/> | For hierarchical and complex designs, identification of the appropriate level for tests and full reporting of outcomes |
| <input checked="" type="checkbox"/> | <input type="checkbox"/> | Estimates of effect sizes (e.g. Cohen's d , Pearson's r), indicating how they were calculated |

Our web collection on [statistics for biologists](#) contains articles on many of the points above.

Software and code

Policy information about [availability of computer code](#)

Data collection Zeiss LSM 710, BD LSR II Flow Cytometer, PerkinElmer IVIS Spectrum, S6 FluoroSpot Analyzer, Infinite M200 plate reader, Bruker Avance III, 400MHz

Data analysis Statistical analysis was performed on Graphpad Prism 7.0, flowcytometry data were analyzed on FlowJo software package (Flowjo V10) and molecular simulation was performed on BIOVIA Discovery Studio 2018;1H NMR spectrum was analyzed by MestReNova x64 (V14.2.0); Confocal images were analyzed by Zen 2011 software.

For manuscripts utilizing custom algorithms or software that are central to the research but not yet described in published literature, software must be made available to editors and reviewers. We strongly encourage code deposition in a community repository (e.g. GitHub). See the Nature Portfolio [guidelines for submitting code & software](#) for further information.

Data

Policy information about [availability of data](#)

All manuscripts must include a [data availability statement](#). This statement should provide the following information, where applicable:

- Accession codes, unique identifiers, or web links for publicly available datasets
- A description of any restrictions on data availability
- For clinical datasets or third party data, please ensure that the statement adheres to our [policy](#)

All data that support the findings of this study are provided within the paper and its Supplementary Information. The raw datasets generated during the study are provided within source data. Source data are provided with this paper. The crystal structure data of TLR7 is accessible in Protein Data Bank (PDB) under the PDB ID: 5GMH.

Field-specific reporting

Please select the one below that is the best fit for your research. If you are not sure, read the appropriate sections before making your selection.

- Life sciences Behavioural & social sciences Ecological, evolutionary & environmental sciences

For a reference copy of the document with all sections, see [nature.com/documents/nr-reporting-summary-flat.pdf](https://www.nature.com/documents/nr-reporting-summary-flat.pdf)

Life sciences study design

All studies must disclose on these points even when the disclosure is negative.

Sample size	No statistical methods were used to determine the sample size in the study. The sample sizes are clearly described in each figure legend. The sample size were determined by allowable error size, accuracy, resources, and need for statistical analysis (generally $n \geq 3$ throughout all the studies) according to the standards of the field.
Data exclusions	No animals and/or data were excluded.
Replication	All experiments were repeated for at least three times and experimental findings were reproducible.
Randomization	The dosing groups were filled by random selection from the same pool of animals for in vivo experiments. Groups in all the in vitro and in vivo experiments were selected randomly.
Blinding	All the investigators were blinded to group allocation during data collection and analysis.

Reporting for specific materials, systems and methods

We require information from authors about some types of materials, experimental systems and methods used in many studies. Here, indicate whether each material, system or method listed is relevant to your study. If you are not sure if a list item applies to your research, read the appropriate section before selecting a response.

Materials & experimental systems

n/a	Involved in the study
<input type="checkbox"/>	<input checked="" type="checkbox"/> Antibodies
<input type="checkbox"/>	<input checked="" type="checkbox"/> Eukaryotic cell lines
<input checked="" type="checkbox"/>	<input type="checkbox"/> Palaeontology and archaeology
<input type="checkbox"/>	<input checked="" type="checkbox"/> Animals and other organisms
<input type="checkbox"/>	<input checked="" type="checkbox"/> Human research participants
<input checked="" type="checkbox"/>	<input type="checkbox"/> Clinical data
<input checked="" type="checkbox"/>	<input type="checkbox"/> Dual use research of concern

Methods

n/a	Involved in the study
<input checked="" type="checkbox"/>	<input type="checkbox"/> ChIP-seq
<input type="checkbox"/>	<input checked="" type="checkbox"/> Flow cytometry
<input checked="" type="checkbox"/>	<input type="checkbox"/> MRI-based neuroimaging

Antibodies

Antibodies used	Anti-mouse CD16/32 antibody (#10131950), APC anti-mouse CD11c antibody (#117309), FITC anti-mouse CD80 antibody (#1104705), PE anti-mouse CD86 antibody (#159203), APC anti-human CD11c antibody (#337207), FITC anti-human CD80 antibody (#375405) and PE anti-human CD86 antibody (#374205) were purchased from Biolegend.
Validation	All antibodies were verified by the supplier and each lot has been quality tested. All the antibodies used are from commercial sources and have been validated by the vendors. Validation data are available on the manufacturer's website.

Eukaryotic cell lines

Policy information about [cell lines](#)

Cell line source(s)	HEK-Blue mTLR7 cells were requested from Prof. Jinjun Shi at Harvard Medical School, who obtained it from InvivoGen (#hkb-mtlr7) and murine macrophage DC2.4 cells were obtained from American Type Culture Collection (ATCC).
Authentication	A short tandem repeat DNA profiling method was used to authenticate the cell lines and the results were compared with reference database. Moreover, no mycoplasma contamination was detected in the above cell lines.
Mycoplasma contamination	All cell lines were tested for mycoplasma contamination. No mycoplasma contamination was found.

Commonly misidentified lines
(See [ICLAC](#) register)

No commonly misidentified cell lines were used.

Animals and other organisms

Policy information about [studies involving animals](#); [ARRIVE guidelines](#) recommended for reporting animal research

Laboratory animals

C57BL/6 mice (female, 6-8 weeks) were ordered from Jackson laboratory and housed in a specific-pathogen-free animal facility at ambient temperature (22 ± 2 °C), air humidity 40%–70% and 12-h dark/12-h light cycle.

Wild animals

No wild animal was used in this study.

Field-collected samples

The study did not involve samples collected from field.

Ethics oversight

All animal experiment protocols were reviewed and approved by the institutional animal care and use committee of the University of Pennsylvania. Animal procedures were performed in accordance with the Guidelines for Care and Use of Laboratory Animals at the University of Pennsylvania.

Note that full information on the approval of the study protocol must also be provided in the manuscript.

Human research participants

Policy information about [studies involving human research participants](#)

Population characteristics

38-year-old healthy male. Other characteristics were not disclosed due to the privacy.

Recruitment

The participant for blood donation was recruited by volunteering.

Ethics oversight

Institutional Review Board of University of Pennsylvania approved pre-clinical studies of the human immune system.

Note that full information on the approval of the study protocol must also be provided in the manuscript.

Flow Cytometry

Plots

Confirm that:

- The axis labels state the marker and fluorochrome used (e.g. CD4-FITC).
- The axis scales are clearly visible. Include numbers along axes only for bottom left plot of group (a 'group' is an analysis of identical markers).
- All plots are contour plots with outliers or pseudocolor plots.
- A numerical value for number of cells or percentage (with statistics) is provided.

Methodology

Sample preparation

Spleens were collected, processed, filtered using a 70 μ m cell strainers in complete RPMI-1640, centrifuged, and red blood cells lysed in ACK lysis buffer. Single-cell suspensions were obtained and stained with antibodies according to the manufacturer's protocols, and then analyzed by flow cytometry.

Instrument

BD LSR II

Software

FlowJo software package (Flowjo V10)

Cell population abundance

The absolute cells $\geq 500,000$ were analyzed for fluorescent intensity in the defined gate.

Gating strategy

In general, cells were first gated on FSC/SSC. Singlet cells were gated using FSC-H and FSC-A. Dead cells were then excluded and further surface and intracellular antigen gating was performed on the live cell population (See supplementary information).

- Tick this box to confirm that a figure exemplifying the gating strategy is provided in the Supplementary Information.